Electronic Supplementary Information

Cobalt corroles with phosphonic acid pendants as catalysts for oxygen and hydrogen evolution from neutral aqueous solution

Huiling Sun,‡[a] Yongzhen Han,‡[a] Haitao Lei,[a] Mingxing Chen,[a] and Rui Cao*[ab]

[a]Department of Chemistry, Renmin University of China, Beijing 100872 China.

[b]School of Chemistry and Chemical Engineering, Shaanxi Normal University, Xi'an 710119 China.

‡These authors contributed equally to this work.

*Correspondence e-mail: ruicao@ruc.edu.cn

General Methods and Materials.

Manipulations of air- and moisture-sensitive materials were performed under nitrogen using standard Schlenk line techniques. All reagents were purchased from commercial suppliers and used as received unless otherwise noted. Complexes 4,6-dibromodibenzofuran[1] and 4,6-diformyldibenzofuran[2] were synthesized according to the literature methods. Dry solvents, acetonitrile, tetrahydrofuran, diethyl ether, dimethylformamide, and dichloromethane were purified by passage through activated alumina. All aqueous solutions were prepared freshly with Milli-Q water. ^{1}H, ^{13}C, and ^{31}P NMR measurements were made on a Brüker spectrometer operating at 400 or 600 MHz. Electronic absorption spectra were acquired using a Hitachi U-3310 spectrophotometer. High-resolution mass spectra were acquired on a Brüker Fourier Transform Ion Cyclotron Resonance Mass Spectrometer APEX IV. SEM images were recorded using a Hitachi SU8020 cold-emission field emission scanning electron microscope with an accelerating voltage of 1 kV. EDX spectra were obtained using JEM-2100F (UHR). The EDX spectra were collected from three randomly selected areas of each sample with an acceleration voltage of 5 kV. The amount of catalysts loaded on the surface of GC or FTO electrodes was ascertained by ICP-AES using VISTA- MPX ICP-AES.

Synthesis.

Synthesis of L^{Br}-Co. The synthetic route of complex L^{Br}-Co is depicted in Scheme S1.

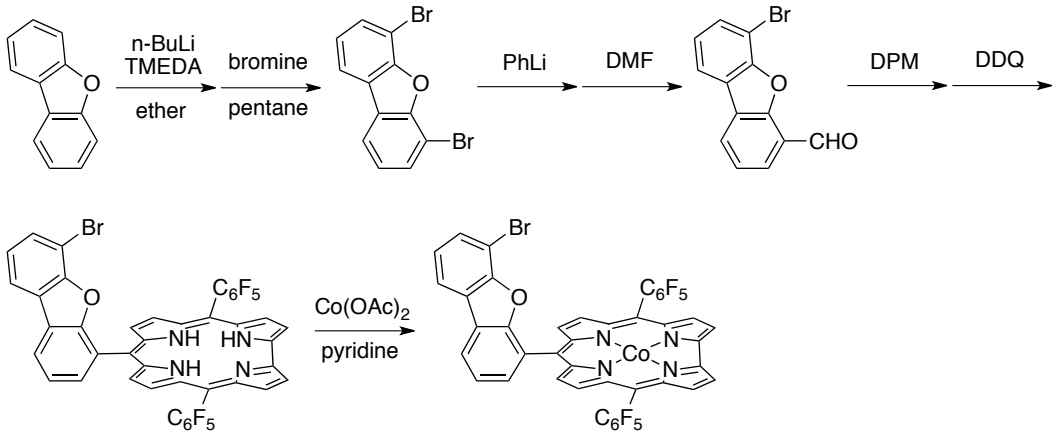

Scheme S1. Synthetic route of complex L^{Br}-Co.

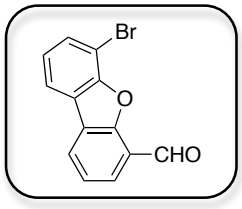

Synthesis of 6-bromo-4-formyldibenzofuran. To a dry THF (600 mL) solution of 4,6-dibromodibenzofuran (9.71 g, 30 mmol) under nitrogen and −78 °C, phenyl lithium (16.4 mL, 31 mmol) was added slowly, and the mixture was kept stirring at −78 °C for 1 h. DMF (15.3 mL, 190 mol) was then added, and the mixture was kept stirring at room temperature for 2 h. The reaction was quenched with addition of 100 mL of water. The resulted mixture was extracted with DCM, dried over Na_2SO_4, and concentrated to dryness using rotavap. The crude product was subjected to silica chromatography (hexane:DCM = 2:1) to afford the fluffy white crystal (5.78 g, 70%). ^{1}H NMR (400 MHz, $CDCl_3$): δ = 10.66 (s, 1H), 8.14 (d, 1H), 7.98 (d, 1H), 7.85 (d, 1H), 7.65 (d, 1H), 7.45 (t, 1H), 7.25 (t, 1H) (Fig. S3). ^{13}C NMR (100 MHz, $CDCl_3$): δ = 187.57, 156.25, 153.77, 131.15,

127.05, 126.96, 125.93, 124.88, 124.46, 123.60, 121.49, 119.91, 104.97 (Fig. S4). HRMS of $[M+Na]^+$: calcd for $C_{13}H_7BrO_2Na$, 296.9527; found, 296.9527 (Fig. S5).

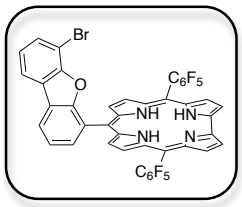

Synthesis of 10-(4-(6-bromodibenzofuran))-5,15-bis(pentafluoro -phenyl)corrole L^{Br}. To a methanol solution (32 mL) of 6-bromo-4-formyldibenzofuran (87.7 mg, 0.32 mmol) and 5-(pentafluorophenyl)dipyrromethane (199.8 mg, 0.64 mmol), was added HCl (1.6 mL, 36%). The solution was stirred at room temperature for 24 h, and was then extracted with $CHCl_3$ (160 mL). The organic phase was separated and washed with water, dried over Na_2SO_4, and was added 2,3-dichloro-5,6-dicyano-1,4-benzoquinone (217.9 mg, 0.96 mmol). The resulted solution was stirred at room temperature for 24 h. The crude product was subjected to silica chromatography (hexane:DCM = 7:1) to afford dark solid (97.0 mg, 35%). Recrystallization from hexane afforded purple crystals. ^{1}H NMR (400 MHz, $CDCl_3$): δ = 9.12 (d, 2H), 8.71 (d, 2H), 8.62 (d, 2H), 8.58 (d, 2 H), 8.36 (d, 1H), 8.26 (d, 1H), 8.11 (d, 1H), 7.82 (t, 1H), 7.53 (d, 1H), 7.31 (t, 1H) (Fig. S6).

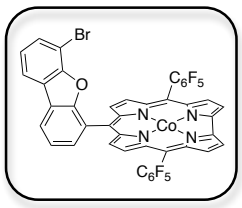

Synthesis of L^{Br}-Co. The mixture of L^{Br} (87.4 mg, 0.10 mmol) in 10 mL pyridine was treated with $Co(OAc)_2{\cdot}4H_2O$ (124.5 mg, 0.50 mmol). The reaction mixture was kept stirring and refluxing for 20 min. The pyridine was then removed under reduced pressure, and the resulting dark solid was dissolved in DCM and washed with water. The organic phase was concentrated to dryness and was subjected to silica chromatography (hexane:DCM = 5:1, containing 1% pyridine) to afford dark green solid (74.4 mg, 80%). ^{1}H NMR (400 MHz, $CDCl_3$): δ = 9.48 (d, 2H), 9.14 (d, 2H), 9.05 (d, 2H), 8.97 (s, 2H), 8.35 (d, 1H),

8.04 (d, 1H), 7.74 (d, 1H), 7.60 (t, 1H), 7.31 (d, 1H), 6.91 (t, 1H), 4.86 (brs, 2H), 4.39 (brs, 4H), 0.98 (brs, 4H) (Fig. S7). HRMS of $[M\text{-}2pyridine]^+$: calcd for $C_{43}H_{14}BrCoF_{10}N_4O$, 929.9523; found, 929.9515 (Fig. S8). Anal. Calcd for M: C, 58.42; H, 2.22; N, 7.71. Found: C, 58.08; H, 2.02; N, 7.43.

Synthesis of L^{COOH}-Co. The synthetic route of complex L^{COOH}-Co is depicted in Scheme S2.

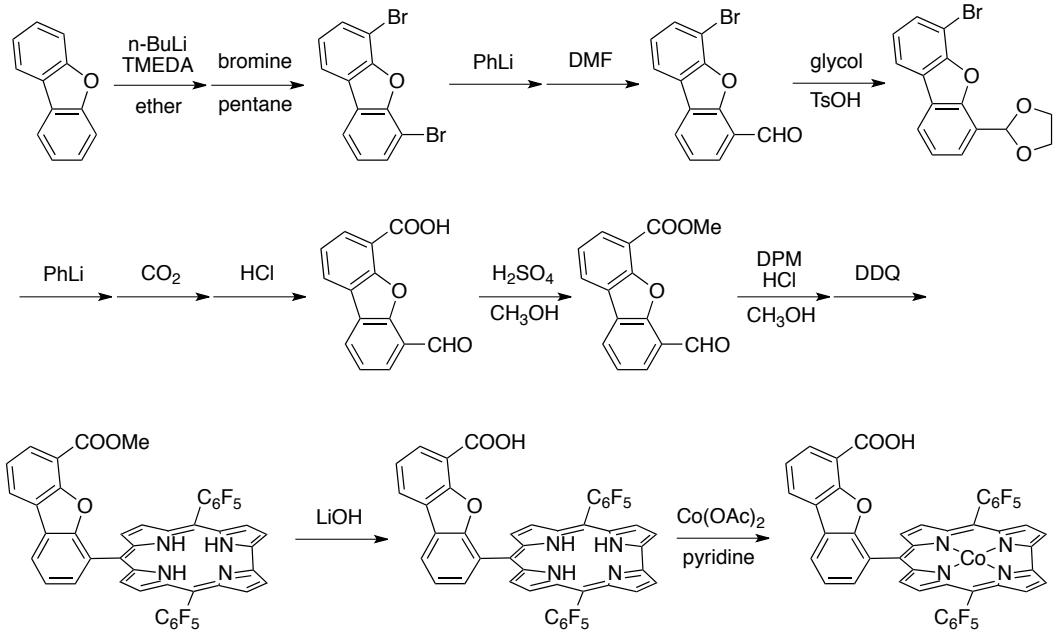

Scheme S2. Synthetic route of complex L^{COOH}-Co.

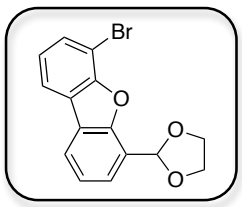

Synthesis of 6-bromo-4-(1,3-dioxolan-2-yl)dibenzofuran. To a 40 mL toluene, was added 6-bromo-4-formyldibenzofuran (5.48 g, 20 mmol), ethylene glycol (4.96 g, 80 mmol), *p*-methylbenzene sulfonic acid (38.0 mg, 0.20 mmol). The solution was stirred under reflux for 2 h under nitrogen. After cooling to room temperature, the resulting mixture was extracted with ethyl acetate, and the organic phase was washed successively with saturated $NaHBO_3$ solution and water, dried over Na_2SO_4, and was concentrated to

dryness under reduced pressure. The crude product was subjected to silica chromatography (hexane:DCM = 1:1) to afford white solid (6.06 g, 95%). ^{1}H NMR (400 MHz, $CDCl_3$): δ = 7.93 (d, 1H), 7.86 (d, 1H), 7.63 (d, 1H), 7.61 (d, 1H), 7.37 (t, 1H), 7.22 (t, 1H), 6.43 (s, 1H), 4.36 (m, 2H), 4.17 (m, 2H) (Fig. S9). ^{13}C NMR (100 MHz, $CDCl_3$): δ = 153.86, 153.53, 130.29, 126.01, 125.44, 124.96, 124.16, 123.24, 123.18, 122.06, 119.73, 104.77, 100.80, 65.99 (Fig. S10). HRMS of $[M+H]^+$: calcd for $C_{15}H_{12}BrO_3$, 318.9970; found, 318.9969 (Fig. S11).

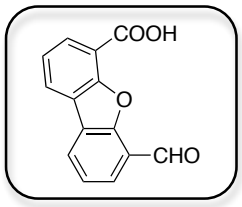

Synthesis of 6-carboxyl-4-formyldibenzofurn. Complex 6-bromo-4-(1,3-dioxolan-2-yl)dibenzofuran (2.38 g, 7.5 mmol) was dissolved in THF (150 mL) under nitrogen. After the solution was cooled to −78 °C, phenyl lithium (4.26 mL, 8.1 mmol, 1.9 M in *n*-butylether) was slowly added. The resulted solution was stirred at −78 °C for 2 h, and was then degassed with a stream of carbon dioxide for 3 h at −78 °C, followed by stirring at room temperature for 2 h. HCl (2 M, 60 mL) was added into the solution with stirring at room temperature for 30 min. THF was removed under reduced pressure, and the resulting crude product was dissolved in methanol followed by filtering to remove the undissolved substance. Concentrating the filtrate to dryness, and the residue was dissolved in DCM and was filtered. The filtrate was concentrated to afford the solid product (1.03 g, 57%), which was directly used in the next step.

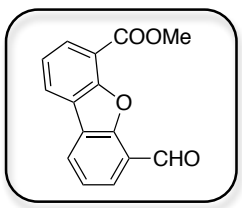

Synthesis of 4-formyl-6-methylacetatedibenzofuran. The solution of 6-carboxyl-4-formyldibenzofurn (960 mg, 4.0 mmol) in methanol (80 mL) was treated with concentrated sulfuric acid (3.2 mL) with stirring under reflux for 4 h. After cooling to room temperature, 80 mL

HCl (2 M) was added with stirring for 30 min. Removing methanol under reduced pressure, and the residue was extracted with DCM, and was dried over Na_2SO_4. The resulting crude product was subjected to silica chromatography (DCM) to afford white powder (1.01 g, 99%). ^{1}H NMR (400 MHz, $CDCl_3$): δ = 10.67 (s, 1H), 8.11 (d, 2H), 8.09 (d, 1H), 7.95 (d, 1H), 7.42 (m, 2H), 4.05 (s, 3H) (Fig. S12). ^{13}C NMR (100 MHz, $CDCl_3$): δ = 187.66, 164.97, 156.63, 155.08, 130.30, 126.87, 126.57, 125.49, 124.87, 124.63, 123.55, 123.34, 121.40, 115.87, 52.51 (Fig. S13). HRMS of $[M+Na]^+$: calcd for $C_{15}H_{10}NaO_4$, 277.0477; found, 277.0472 (Fig. S14).

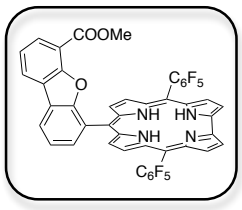

Synthesis of L^{COOMe}. To a methanol solution (320 mL) of 4-formyl-6-methylacetatedibenzofuran (0.81 g, 3.2 mmol) and 5-(pentafluorophenyl)dipyrromethane (1.98 g, 6.4 mmol), was added 16 mL of HCl (36%), and the solution was stirred at room temperature for 8 h. The reaction mixture was then extracted with $CHCl_3$. The organic phase was washed with water, dried over Na_2SO_4, added 2,3-dichloro-5,6-dicyano-1,4-benzoquinone (DDQ, 2.16 g, 9.5 mmol) with stirring at room temperature for 10 h. The solution was then concentrated to dryness and subjected to silica chromatography (hexane:DCM = 1:1) to afford purple solid. Recrystallization from DCM/hexane/pyridine (1:1:0.01) afforded purple diamond crystals (0.80 g, 29%). ^{1}H NMR (400 MHz, $CDCl_3$): δ = 9.10 (s, 2H), 8.62 (m, 6H), 8.32 (m, 3H), 7.96 (d, 1H), 7.82 (t, 1H), 7.43 (t, 1H), 2.92 (s, 3H) (Fig. S15). HRMS of $[M]^+$: calcd for $C_{45}H_{20}F_{10}N_4O_3$, 854.1376; found, 854.1368 (Fig. S16).

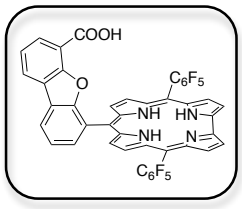

Synthesis of L^{COOH}. To a THF solution (40 mL) of L^{COOH} (0.34 g, 0.4 mmol), was added LiOH (0.48 g, 20 mmol). The solution with stirred under reflux for 4 h, and was then cooled to room temperature. HCl (8 mL, 2 M) was added with stirring, and the THF was removed under reduced pressure. The residue was extracted with DCM, washed with water, and dried over Na_2SO_4. Recrystallization form hexane/DCM (1:1) afforded dark green solid (0.32 g, 95%). ^{1}H NMR (400 MHz, $CDCl_3$): δ = 9.13 (d, 2H), 8.67 (d, 2H), 8.59 (m, 4H), 8.38 (t, 2H), 8.27 (d, 1H), 7.86 (m, 2H), 7.43 (t, 1H) (Fig. S17). HRMS of $[M+Na]^+$: calcd for $C_{44}H_{18}F_{10}N_4NaO_3$, 863.1117; found, 863.1126 (Fig. S18).

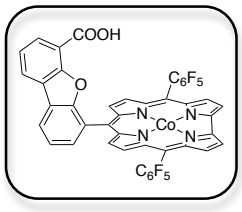

Synthesis of L^{COOH}-Co. L^{COOH} (84.01 mg, 0.10 mmol) in 10 mL of pyridine was treated with $Co(OAc)_2{\cdot}4H_2O$ (124.5 mg, 0.50 mmol), and the solution was stirred under reflux for 20 min. The solvent pyridine was removed under reduced pressure, and the resulting dark solid was dissolved in DCM and washed with water. The organic phase was concentrated to dryness and was subjected to silica chromatography (DCM containing 1% pyridine) to afford dark green solid (75.2 mg, 84%). ^{1}H NMR (400 MHz, $CDCl_3$): δ = 9.25 (d, 2H), 8.86 (d, 2H), 8.77 (m, 4H), 8.35 (d, 1H), 8.29 (d, 1H), 8.13 (d, 1H), 7.94 (d, 1H), 7.76 (d, 1H), 7.44 (t, 1H), 5.90 (brs, 2H), 5.06 (brs, 4H), 1.75(brs, 4H) (Fig. S19). HRMS of $[M\text{-}2pyridine+Na]^+$: calcd for $C_{44}H_{15}CoF_{10}N_4NaO_3$, 919.0214; found, 919.0210 (Fig. S20). Anal. Calcd for M: C, 61.49; H, 2.39; N, 7.97. Found: C, 61.11; H, 2.15; N, 7.58.

Synthesis of $L^{PO(OH)_2}$-Co. The synthetic route of complex $L^{PO(OH)_2}$-Co is depicted in Scheme S3.

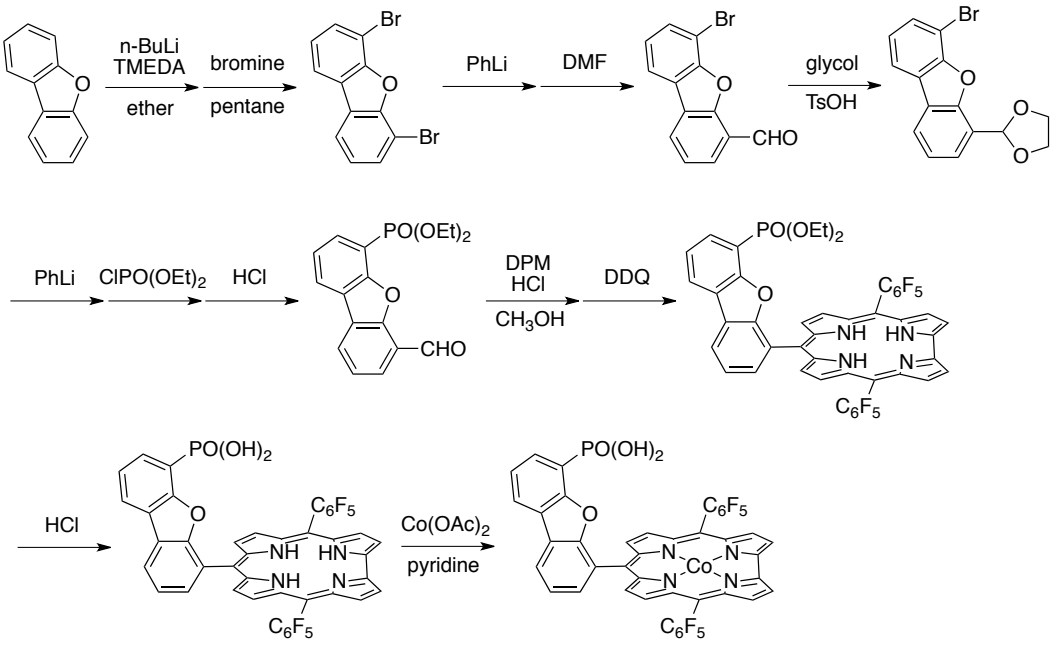

Scheme S3. Synthetic route of complex $L^{PO(OH)_2}$-Co.

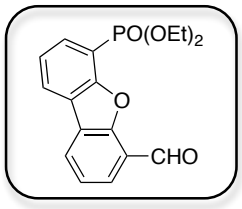

Synthesis of 4-formyl-6-diethylphosphonate-dibenzofuran. To a dry THF solution (150 mL) of 6-bromo-4-(1,3-dioxolan-2-yl) dibenzofuran (2.38 g, 7.5 mmol), was added phenyl lithium (4.26 mL, 8.1 mmol, 1.9 M in *n*-butyl ether) at −78 °C. The resulting solution was stirred at this temperature for 2 h, and diethyl chlorophosphate (1.35 g, 7.8 mmol) was added with stirring. The solution was then stirred at room temperature for 2 h, and 60 mL of HCl (2 M) was added. THF was removed under reduced pressure, and the residue was extracted with DCM and dried over Na_2SO_4. The organic phase was concentrated to dryness and subjected to silica chromatography (DCM:ethyl acetate = 4:1) to afford white solid (1.06 g, 43%). ^{1}H NMR (400 MHz, $CDCl_3$): δ = 10.67 (s, 1H), 8.16 (m, 2H), 7.98 (m, 2H), 7.47 (m, 2H), 4.28 (m, 4H), 1.37 (t, 6H) (Fig. S21).

^{13}C NMR (100 MHz, $CDCl_3$): δ = 187.42, 156.51, 156.44, 132.78, 132.73, 126.96, 126.78, 125.34, 125.01, 123.68, 123.56, 123.40, 121.37, 62.90, 62.84, 16.54, 16.47 (Fig. S22). ^{31}P NMR (400 MHz, $CDCl_3$): δ = 13.2 (s, 1P) (Fig. S23). HRMS of $[M+Na]^+$: calcd for $C_{17}H_{17}NaO_5P$, 355.0711; found, 355.0706 (Fig. S24).

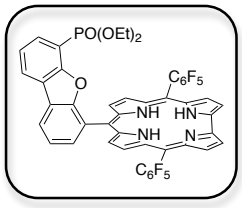

Synthesis of $L^{PO(OEt)_2}$. To a methanol solution (320 mL) of 4-formyl-6-diethylphosphonate-dibenzofuran (1.06 g, 3.2 mmol) and 5-(pentafluorophenyl)dipyrromethane (1.99 g, 6.4 mmol), was added 16 mL of HCl (2 M). The solution was stirred at room temperature for 10 h, and was extracted with $CHCl_3$. The organic phase was washed with water, dried over Na_2SO_4, and was added with DDQ (2.16 g, 9.5 mmol). The resulting solution was stirred at room temperature for 10 h, and was then concentrated to dryness and subjected to silica chromatography (DCM:ethyl acetate = 20:1) to afford purple solid. Recrystallization from DCM/hexane (1:1) afforded purple diamond crystals (1.50 g, 50%). ^{1}H NMR (400 MHz, $CDCl_3$): δ = 9.11 (d, 2H), 8.66 (d, 2H), 8.57 (m, 4H), 8.37 (m, 2H), 8.18 (d, 1H), 7.76 (m, 2H), 7.48 (t, 1H), 3.17 (m, 2H), 3.11 (m, 2H), 1.24 (m, 6H) (Fig. S25). ^{31}P NMR (400 MHz, $CDCl_3$): δ = 12.52 (s, 1P) (Fig. S26). HRMS of $[M+Na]^+$: calcd for $C_{47}H_{27}F_{10}N_4NaO_4P$, 955.1508; found, 955.1498 (Fig. S27).

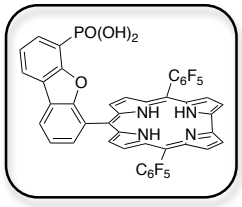

Synthesis of $L^{PO(OH)_2}$. $L^{PO(OEt)_2}$ (186 mg, 0.20 mmol) was treated with 20 mL of concentrated hydrochloric acid with stirring under reflux at 115 °C for 24 h. After cooling to room temperature, the resulting reaction mixture was extracted with DCM, and the organic phase was washed with water and dried over Na_2SO_4. The product was collected by filtration to give dark green solid (160 mg, 91%). ^{1}H NMR (400 MHz, $CDCl_3$): δ = 9.17 (d, 2H),

8.67 (d, 2H), 8.60 (d, 2H), 8.58 (d, 2H), 8.41 (t, 2H), 8.23 (d, 1H), 7.91 (m, 1H), 7.84 (m, 2H) (Fig. S28). ^{31}P NMR (600 MHz, $CDCl_3$): δ = 2.88 (s, 1P) (Fig. S29). HRMS of $[M+Na]^+$: calcd for $C_{43}H_{19}F_{10}N_4NaO_4P$, 899.0882; found, 899.0879 (Fig. S30).

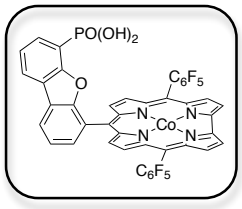

Synthesis of $L^{PO(OH)_2}$-Co. The solution of $L^{PO(OH)_2}$ (87.6 mg, 0.10 mmol) in 10 mL of pyridine was treated with $Co(OAc)_2{\cdot}4H_2O$ (124.5 mg, 0.50 mmol) and was stirred under reflux for 20 min. The solvent pyridine was removed under reduced pressure, and the resulting dark solid was re-dissolved by DCM. The organic phase was washed with water, dried over Na_2SO_4. The crude product was subjected to silica chromatography (DCM:methanol = 5:1 containing 1% pyridine) to afford dark green solid (85 mg, 91%). ^{1}H NMR (400 MHz, CD_2Cl_2): δ = 8.16 (s, 2H), 7.74 (d, 2H), 7.59 (d, 2H), 7.09 (d, 2H), 6.89 (d, 1H), 6.77 (d, 1H), 6.69 (d, 2H), 6.47 (d, 1H), 6.32 (s, 1H), 4.23(m, 4H) (Fig. S31). ^{31}P NMR (600 MHz, CD_2Cl_2): δ = −19.6 (s, 1P) (Fig. S32). HRMS of $[M\text{-}2pyridine+Na]^+$: calcd for $C_{43}H_{16}CoF_{10}N_4NaO_4P$, 954.9979; found, 954.9977 (Fig. S33). Anal. Calcd for M: C, 58.36; H, 2.40; N, 7.71. Found: C, 58.03; H, 2.21; N, 7.53.

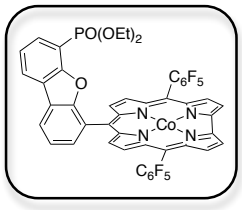

Synthesis of *$L^{PO(OEt)_2}$-Co.* The solution of $L^{PO(Et)_2}$ (93.2 mg, 0.10 mmol) in 10 mL of pyridine was treated with $Co(OAc)_2{\cdot}4H_2O$ (124.5 mg, 0.50 mmol) and was stirred under reflux for 20 min. The solvent pyridine was removed under reduced pressure, and the resulting dark solid was re-dissolved by DCM. The organic phase was washed with water and dried over Na_2SO_4. The crude product was subjected to silica chromatography (DCM:methanol = 5:1 containing 1% pyridine) to afford dark green solid (92 mg,

93%). ^{1}H NMR (400 MHz, $CDCl_3$): δ = 9.26 (d, 2H), 8.80 (d, 2H), 8.71 (m, 4H), 8.42 (d, 1H), 8.35 (d, 1H), 7.95 (m, 1H), 7.83 (d, 1H), 7.67 (t, 1H), 7.55 (m, 1H), 6.06 (brs, 2H), 5.13 (brs, 4H), 3.35 (m, 2H), 3.24 (m, 2H), 1.62 (brs, 4H), 0.43 (t, 6H) (Fig. S34). ^{31}P NMR (400 MHz, $CDCl_3$): δ = 14.22 (s, 1P) (Fig. S35). HRMS of $[M\text{-}2pyridine+Na]^+$: calcd for $C_{47}H_{24}CoF_{10}N_4NaO_4P$, 1011.0605; found, 1011.0708 (Fig. S36).

Synthesis of $L^{CH_2PO(OH)_2}$-Co. The synthetic route of complex $L^{CH_2PO(OH)_2}$-Co is depicted in Scheme S4.

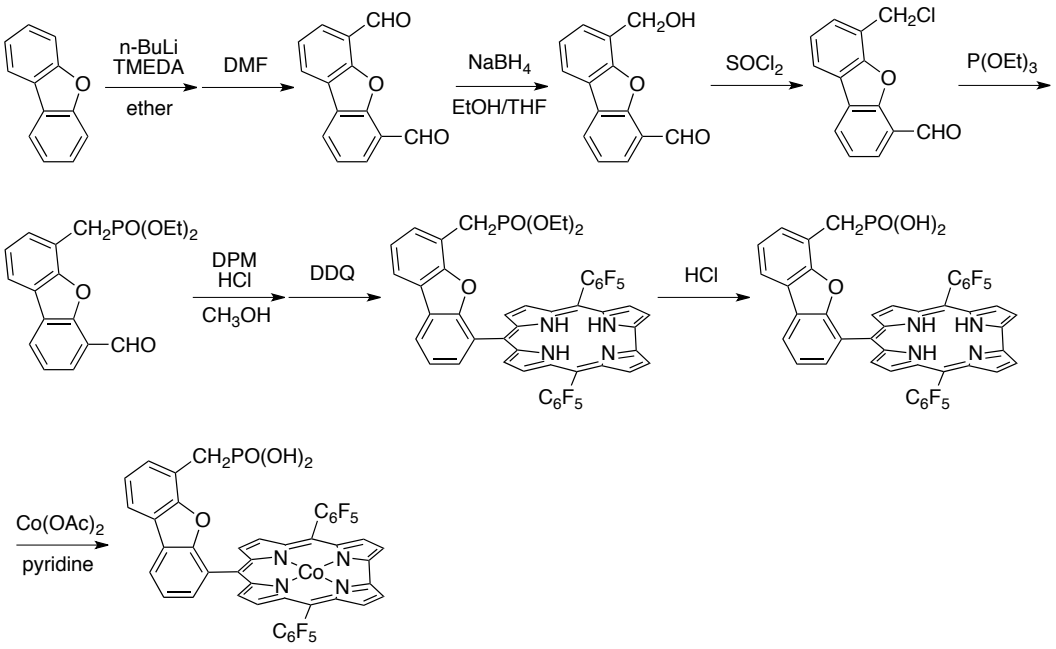

Scheme S4. Synthetic route of complex $L^{CH_2PO(OH)_2}$-Co.

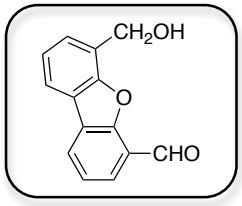

Synthesis of 4-formyl-6-hydroxymethyldibenzofuran. To a mixture solution of ethanol (175 mL) and THF (250 mL) containing 4,6-diformyldibenzofuran (2.24 g, 10 mmol) at −5 °C, was added $NaBH_4$ (94.7 mg, 2.5 mmol). The resulting solution was stirred at −5 °C for 30 min, and was kept stirring at 0 °C for 7 h. The solution became green, and 2 M

HCl was added to adjust the pH to 5. The solvent was removed under reduced pressure, and the resulting residue was extracted with DCM. The organic phase was washed with water and dried over Na_2SO_4, and was then concentrated to dryness and subjected to silica chromatography (DCM:ethyl acetate = 10:1) to afford the solid product (1.28 g, 57%). ^{1}H NMR (400 MHz, $CDCl_3$): δ = 10.46 (s, 1H), 8.07 (dd, 1H), 7.86 (dd, 1H), 7.79 (dd, 1H), 7.55 (d, 1H), 7.40 (t, 1H), 7.34 (t, 1H), 5.09 (d, 2H), 3.50 (t, 1H) (Fig. S38).

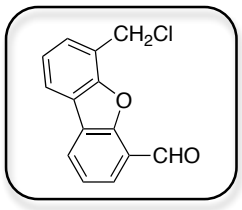

Synthesis of 4-formyl-6-chloromethyldibenzofuran. To a DCM (40 mL) of 4-formyl-6-hydroxymethyldibenzofuran (0.90 g, 4 mmol), was added pyridine (0.32 g, 4 mmol) and $SOCl_2$ (0.48 g, 4 mmol). The solution was stirred under reflux for 4 h, and then was washed with saturated NaCl, and dried over Na_2SO_4. The organic phase was concentrated to dryness and subjected to silica chromatography (petroleum ether:DCM = 2:1) to afford the yellow solid product (0.63 g, 64%). ^{1}H NMR (400 MHz, $CDCl_3$): δ = 10.71 (s, 1H), 8.21 (d, 1H), 8.00 (m, 2H), 7.61 (d, 1H), 7.51 (t, 1H), 7.44 (t, 1H), 5.05 (s, 2H) (Fig. S39).

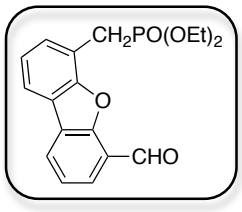

Synthesis of 4-formyl-6-diethylphosphatemethyldibenzofuran. Complex 4-formyl-6-chloromethyldibenzofuran (0.37 g, 1.5 mmol) was added to 1.5 mL of triethyl phosphite. The solution was stirred under reflux for 3 h, and the solvent triethyl phosphite was removed under reduced pressure, and the crude product was subjected to silica chromatography (DCM:ethyl acetate = 10:1) to afford the white oily product (0.38 g, 73%). ^{1}H NMR

(400 MHz, $CDCl_3$): δ = 10.51(s, 1H), 8.03 (d, 1H), 7.83 (d, 1H), 7.75 (d, 1H), 7.46 (d, 1H), 7.34 (t, 1H), 7.27 (t, 1H), 4.03 (m, 4H), 3.50 (d, 2H), 1.13 (t, 6H) (Fig. S40).

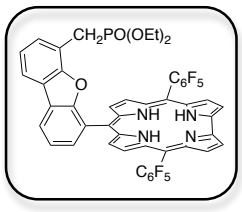

Synthesis of $L^{CH_2PO(OEt)_2}$. To a mixture solvent of methanol (90 mL) and water (90 mL), was added complex 4-formyl-6-diethylphosphatemethyldibenzofuran (0.31 g, 0.9 mmol) and 5-(pentafluorophenyl)dipyrromethane (0.56 g, 1.8 mmol). HCl (4.5 mL, 36%) was added, and the solution was stirred at room temperature for 7 h, and was then extracted with $CHCl_3$. The organic phase was washed with water and dried over Na_2SO_4. A sample of DDQ (0.62 g, 2.7 mmol) was added, and the solution was stirred at room temperature for 10 h. The solution was concentrated to dryness and was subjected to silica chromatography (DCM:ethyl acetate = 50:1) to afford purple solid (0.36 g, 42%). ^{1}H NMR (400 MHz, $CDCl_3$): δ = 9.14 (d, 2H), 8.67 (d, 2H), 8.59 (m, 4H), 8.39 (d, 1H), 8.20 (d, 1H), 8.09 (d, 1H), 7.79 (t, 1H), 7.38 (t, 1H), 7.32 (d, 1H), 3.28 (m, 4H), 2.76 (d, 2H), 0.56 (t, 6H) (Fig. S41). HRMS of $[M+H]^+$: calcd for $C_{48}H_{30}F_{10}N_4O_4P$, 947.1845; found, 947.1839 (Fig. S42).

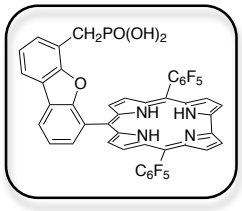

Synthesis of $L^{CH_2PO(OH)_2}$. Ligand precursor $L^{CH_2PO(OEt)_2}$ (67 mg, 0.07 mmol) was treated with 6 mL of concentrated hydrochloric acid, and the mixture was stirred under reflux for 12 h. After cooling to room temperature, the resulting reaction mixture was extracted with DCM, and the organic phase was washed with saturated sodium chloride and dried over

Na_2SO_4. The crude product was subjected to silica chromatography (DCM:ethyl acetate = 20:1) to afford purple solids (47 mg, 75%). ^{1}H NMR (400 MHz, $CDCl_3$): δ = 8.89 (s, 2H), 8.53 (s, 2H), 8.33 (d, 4H), 8.11 (d, 1H), 7.89 (m, 2H), 7.64 (d, 1H), 7.55 (t, 1H), 6.85 (s, 1H), 2.88 (d, 2H) (Fig. S43). ^{31}P NMR (600 MHz, $CDCl_3$): δ = 15.5 (s, 1P) (Fig. S44). HRMS of $[M+H]^+$: calcd for $C_{44}H_{22}F_{10}N_4O_4P$, 891.1219; found, 891.1218 (Fig. S45).

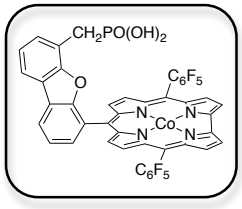

Synthesis of $L^{CH_2PO(OH)_2}$*-Co.* To 4.5 mL of pyridine solution of $L^{CH_2PO(OH)_2}$ (40.1 mg, 0.045 mmol), was added $Co(OAc)_2{\cdot}4H_2O$ (56 mg, 0.225 mmol). The solution was stirred under reflux for 20 min, and the pyridine solvent was removed under reduced pressure. The resulting dark solid was re-dissolved in DCM, and the organic phase was washed with water, dried over Na_2SO_4. The crude product was subjected to silica chromatography (ethyl acetate:methanol = 4:1 containing 1% pyridine) to afford purple solids (30 mg, 72%). ^{1}H NMR (400 MHz, CD_2Cl_2): δ = 9.61 (m, 2H), 9.36 (m, 2H), 8.75 (m, 4H), 8.41 (m, 1H), 8.22 (m, 1H), 7.95 (m, 1H), 7.74 (m, 1H), 7.42 (m, 1H), 6.84 (m, 1H), 3.68 (m, 2H), 3.43 (m, 4H) (Fig. S46). ^{31}P NMR (600 MHz, CD_2Cl_2): δ = −13.4 (s, 1P) (Fig. S47). HRMS of $[M\text{-}2pyridine+H]^+$: calcd for $C_{44}H_{19}CoF_{10}N_4O_4P$, 947.0316; found, 947.0318 (Fig. S48). Anal. Calcd for M: C, 58.71; H, 2.56; N, 7.61. Found: C, 58.58; H, 2.32; N, 7.33.

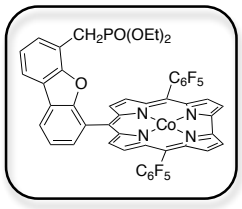

Synthesis of $L^{CH_2PO(OEt)_2}$*-Co.* To 5 mL of pyridine solution of $L^{CH_2PO(OEt)_2}$ (47.3 mg, 0.05 mmol), was added $Co(OAc)_2 \cdot 4H_2O$ (62 mg, 0.25 mmol). The solution was stirred under reflux for 20 min. The pyridine solvent was removed under reduced pressure, and the resulting solid was re-dissolved in DCM. The organic phase was washed with water, dried over Na_2SO_4. The crude product was subjected to silica chromatography (DCM) to afford purple solids. Recrystallization from DCM/hexane/pyridine (1:5:0.06) afforded sheet purple plates (36 mg, 72%). ^{1}H NMR (400 MHz, $CDCl_3$): δ = 9.24 (d, 2H), 8.84 (d, 2H), 8.77 (d, 2H), 8.69 (d, 2H), 8.28 (dd, 1H), 8.09 (dd, 1H), 8.03 (m, 1H), 7.69 (t, 1H), 7.32 (d, 2H), 6.01 (brs, 2H), 5.08 (brs, 4H), 3.35 (m, 4H), 2.46 (d, 2H), 1.28 (brs, 4H), 0.77 (t, 6H) (Fig. S49). HRMS of $[M\text{-}2pyridine+Na]^+$: calcd for $C_{48}H_{26}CoF_{10}N_4NaO_4P$, 1025.0762; found, 1025.0750 (Fig. S50).

Electrochemical Studies.

All electrochemical experiments were carried out using a CH Instruments (model CHI660D Electrochemical Analyzer) at 20 °C, and the solution was bubbled with N_2 for at least 30 min before analysis. CVs were acquired in 5 mL of dry acetonitrile (0.1 M *n*-Bu_4NPF_6) containing 0.5 mM of Co corroles and used a three-compartment cell with a 0.07 cm^2 glassy carbon (GC) electrode as the working electrode, Ag/Ag^+ as the reference electrode, and Pt wire as the auxiliary electrode. The working electrode was polished with α-Al_2O_3 of decreasing sizes (0.3 μm to 50 nm) and washed with distilled H_2O and absolute ethanol. LSVs were acquired in 0.1

M pH 7 phosphate buffer and used a three-compartment cell with a catalyst-coated GC (0.07 cm^2) or FTO (0.25 cm^2) electrode as the working electrode, Ag/AgCl as the reference electrode, and Pt wire as the auxiliary electrode. The catalyst-coated GC electrodes were prepared by dropping directly 5 μL of DCM solution containing 1 mM catalyst onto the GC electrode surface. Slow evaporation at room temperature gives a thin film with 70 nmol of the catalyst per square centimeter. The catalyst-coated FTO electrodes were prepared by dropping directly 5 μL of DCM solution containing 1 mM catalyst onto a FTO. Slow evaporation at room temperature gives a thin film with 20 nmol of the catalyst per square centimeter. Controlled potential electrolysis recorded in 0.1 M pH 7 phosphate buffer was measured at 1.5 V in a three-compartment cell with a catalyst-coated GC electrode as the working electrode, Ag/AgCl as the reference electrode, and Pt wire as the auxiliary electrode. Analysis of O_2 produced in CPE experiments was conducted by using a calibrated Ocean Optics FOXY probe (Model NeoFox). Background from the buffer-only solution was measured in the same method and was deducted. The H_2 produced during CPE was detected using gas chromatography analysis.

Crystallographic Studies.

Complete data sets for corrole complexes $L^{CH_2PO(OEt)_2}$-Co (CCDC 1526193), $L^{PO(OEt)_2}$ (CCDC 1526195), L^{COOMe} (CCDC 1526194), and L^{Br}-Co-PPh_3 (1526192) were collected. Single crystals suitable for X-ray analysis were each coated with Paratone-N oil, suspended in a small fiber loop, and placed in a cooled gas stream on a Bruker D8 VENTURE X-ray diffractometer. Diffraction intensities were measured

using graphite monochromated Mo Kα radiation (λ = 0.71073 Å). Data collection, indexing, data reduction and final unit cell refinements were carried out using APEX2.[3] Absorption corrections were applied using the program SADABS.[4] The structures were solved with direct methods using SHELXS[5] and refined against F^2 on all data by full-matrix least squares with SHELXL-97[6] following established refinement strategies.

All non-hydrogen atoms were refined anisotropically. All hydrogen atoms binding to carbon were included into the model at geometrically calculated positions and refined using a riding model. The isotropic displacement parameters of all hydrogen atoms were fixed to 1.2 times the U value of the atoms they are linked to (1.5 times for methyl groups). In the structure of $L^{CH_2PO(OEt)_2}$-Co, there is a co-crystallized DCM solvent molecule per molecule of $L^{CH_2PO(OEt)_2}$-Co. Automatic structure evaluation performed with PLATON as implemented in the CheckCIF routine resulted in two level A alerts for the structure of $L^{CH_2PO(OEt)_2}$-Co. These alerts are largely due to the relatively low quality of the crystals, which leads to very few and poor diffraction spots at high-resolution regions. In the structure of $L^{PO(OEt)_2}$, there is a co-crystallized hexane solvent molecule per molecule of $L^{PO(OEt)_2}$. In the structure of L^{COOMe}, there are two molecules of L^{COOMe} in the asymmetric unit. Automatic structure evaluation performed with PLATON as implemented in the CheckCIF routine resulted in one level A alert. This alert concerning solvent accessible voids is a result of the large size of molecules of L^{COOMe} and also the unresolved solvent molecules in the crystal lattice. The calculated voids is only 6.2% of one unit cell volume of L^{COOMe}. Details of the data quality and a summary of the residual values of the refinements are listed in Table S1.

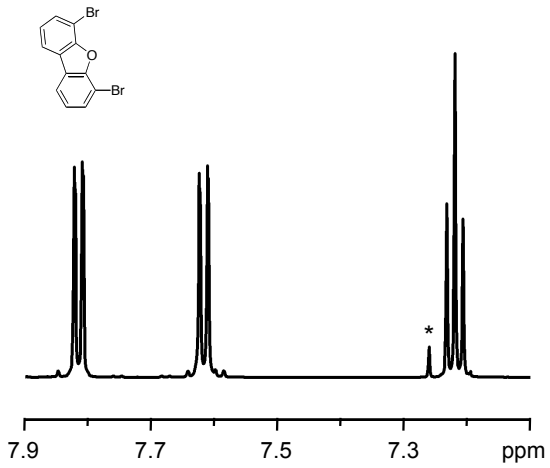

Figure S1. ^{1}H NMR spectrum of 4,6-dibromodibenzofuran in $CDCl_3$. The solvent residue peak of $CDCl_3$ is labeled (*).

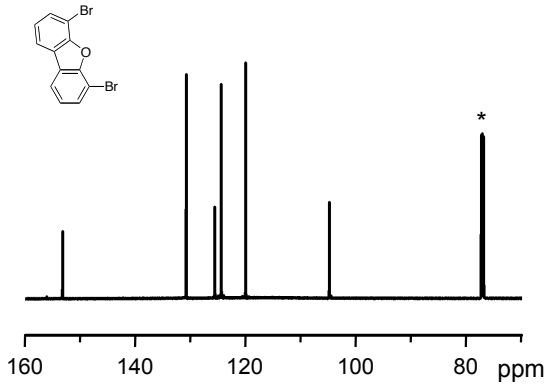

Figure S2. ^{13}C NMR spectrum of 4,6-dibromodibenzofuran in $CDCl_3$. The solvent residue peak of $CDCl_3$ is labeled (*).

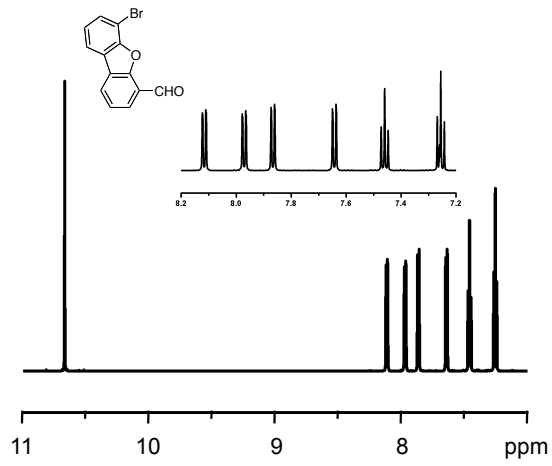

Figure S3. ^{1}H NMR spectrum of 6-bromo-4-formyldibenzofuran in $CDCl_3$.

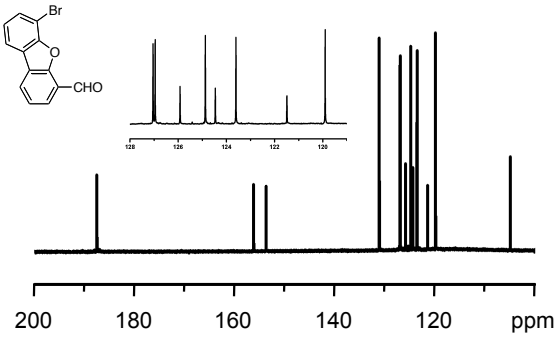

Figure S4. ^{13}C NMR spectrum of 6-bromo-4-formyldibenzofuran in $CDCl_3$.

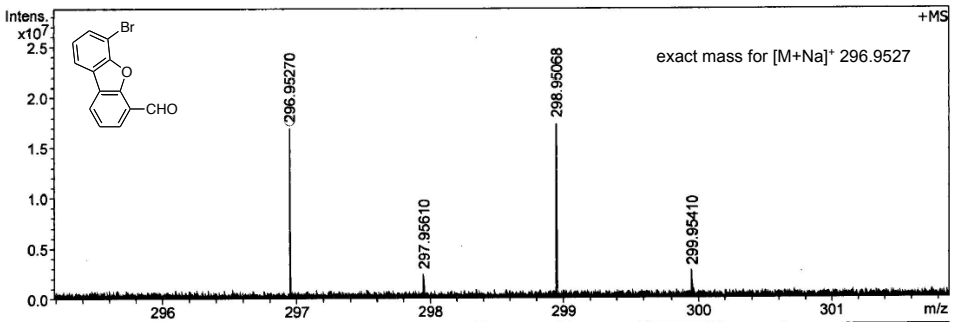

Figure S5. HRMS of 6-bromo-4-formyldibenzofuran.

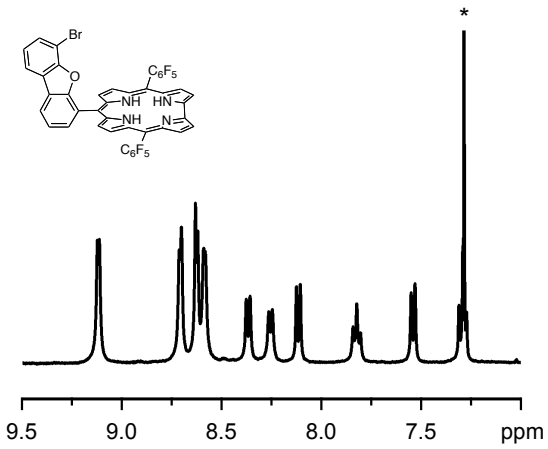

Figure S6. ^{1}H NMR spectrum of L^{Br} in $CDCl_3$. The solvent residue peak of $CDCl_3$ is labeled (*).

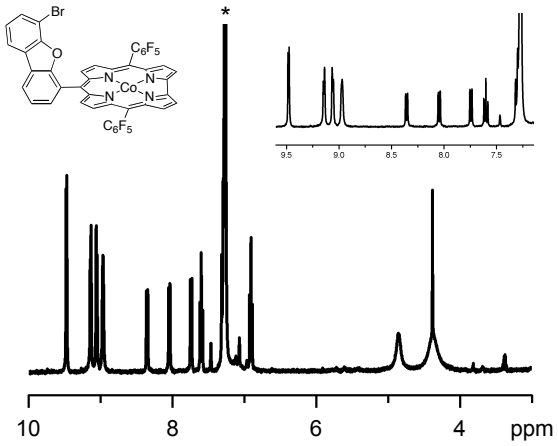

Figure S7. ^{1}H NMR spectrum of L^{Br}-Co in $CDCl_3$. The solvent residue peak of $CDCl_3$ is labeled (*).

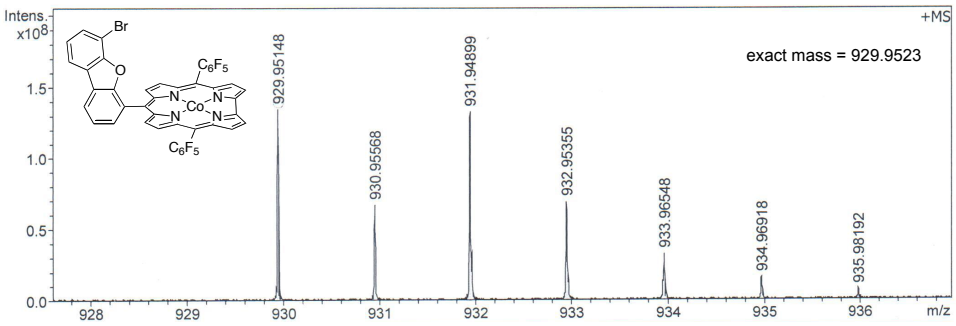

Figure S8. HRMS of L^{Br}-Co.

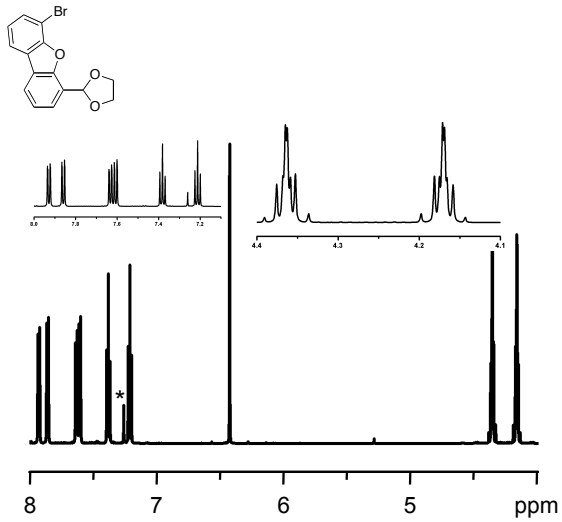

Figure S9. ^{1}H NMR spectrum of 6-bromo-4-(1,3-dioxolan-2-yl)dibenzofuran in $CDCl_3$. The solvent residue peak of $CDCl_3$ is labeled (*).

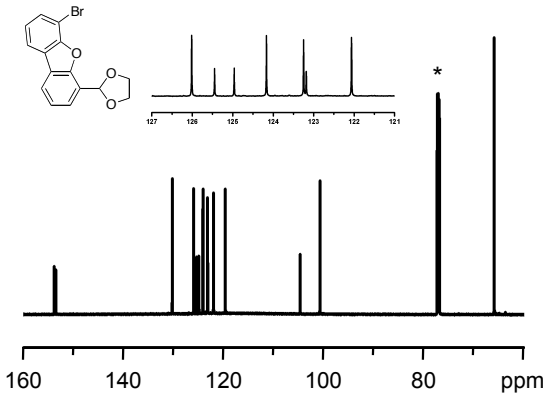

Figure S10. ^{13}C NMR spectrum of 6-bromo-4-(1,3-dioxolan-2-yl)dibenzofuran in $CDCl_3$. The solvent residue peak of $CDCl_3$ is labeled (*).

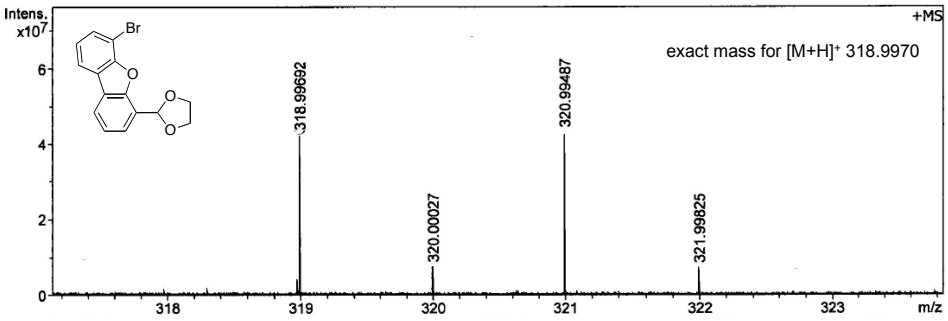

Figure S11. HRMS of 6-bromo-4-(1,3-dioxolan-2-yl)dibenzofuran.

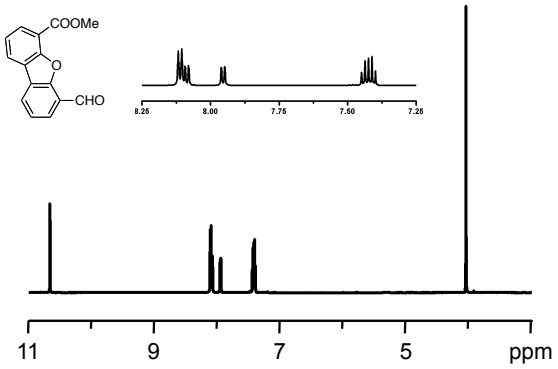

Figure S12. ^{1}H NMR spectrum of 4-formyl-6-methylacetatedibenzofuran in $CDCl_3$.

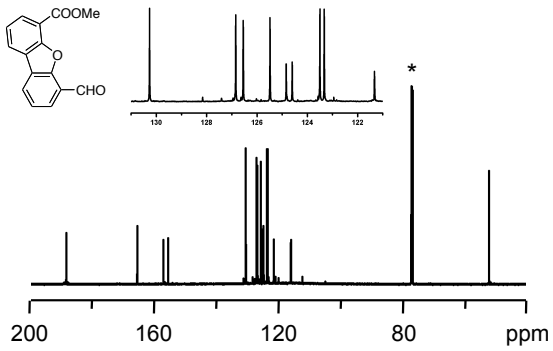

Figure S13. ^{13}C NMR spectrum of 4-formyl-6-methylacetatedibenzofuran in $CDCl_3$. The solvent residue peak of $CDCl_3$ is labeled (*).

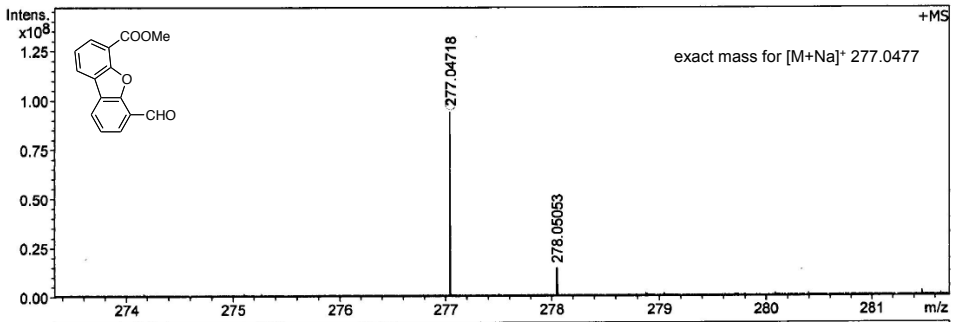

Figure S14. HRMS of 4-formyl-6-methylacetatedibenzofuran.

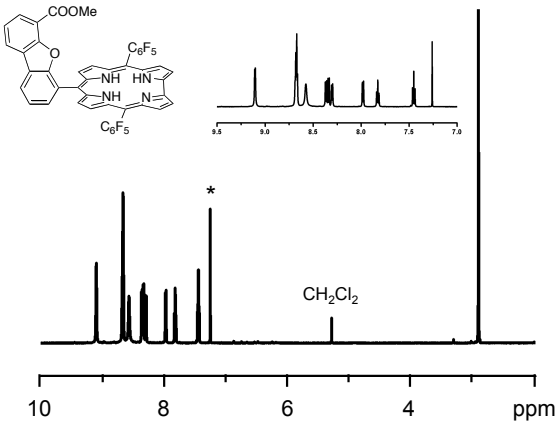

Figure S15. ^{1}H NMR spectrum of L^{COOMe} in $CDCl_3$. The solvent residue peak of $CDCl_3$ is labeled (*).

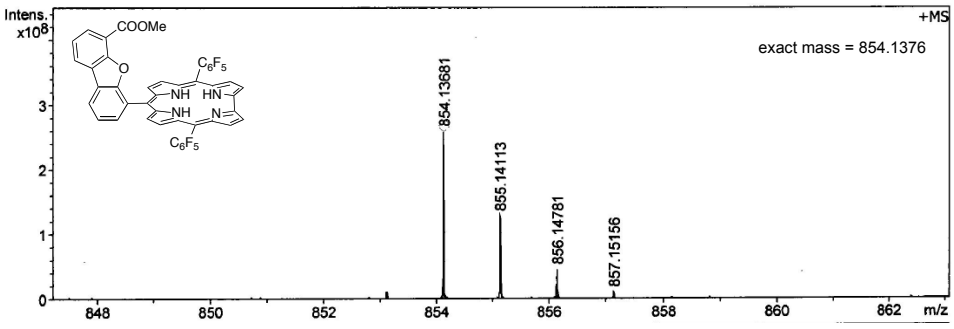

Figure S16. HRMS of L^{COOMe}.

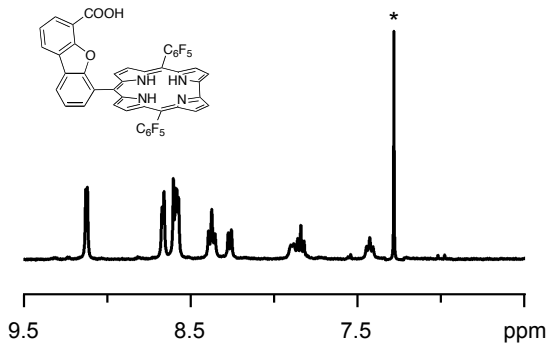

Figure S17. ^{1}H NMR spectrum of L^{COOH} in $CDCl_3$. The solvent residue peak of $CDCl_3$ is labeled (*).

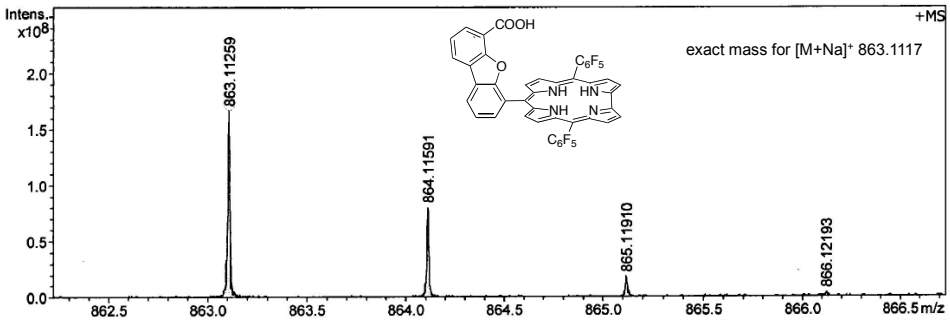

Figure S18. HRMS of L^{COOH}.

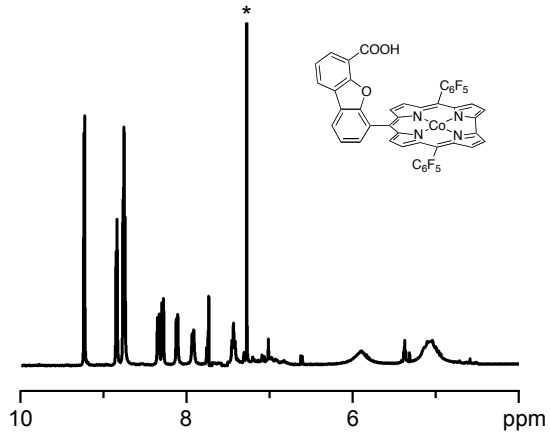

Figure S19. ^{1}H NMR spectrum of L^{COOH}-Co in $CDCl_3$. The solvent residue peak of $CDCl_3$ is labeled (*).

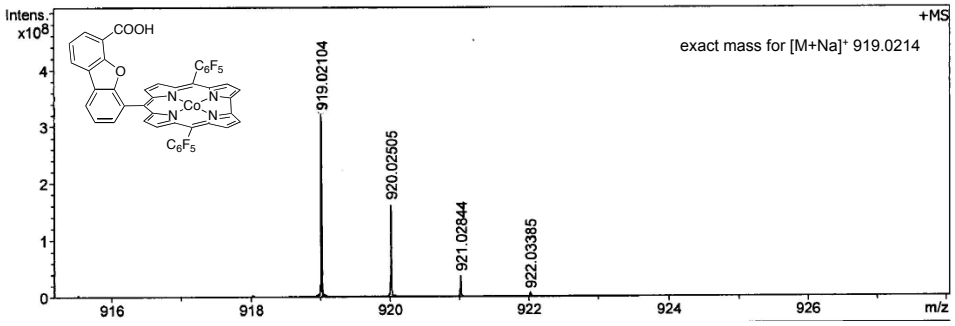

Figure S20. HRMS of L^{COOH}-Co.

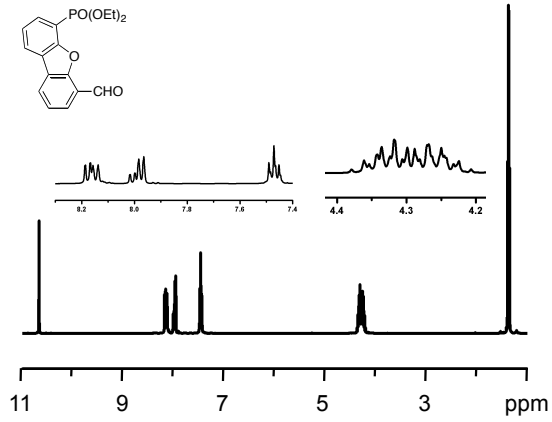

Figure S21. ^{1}H NMR spectrum of 4-formyl-6-diethylphosphonate-dibenzofuran in $CDCl_3$.

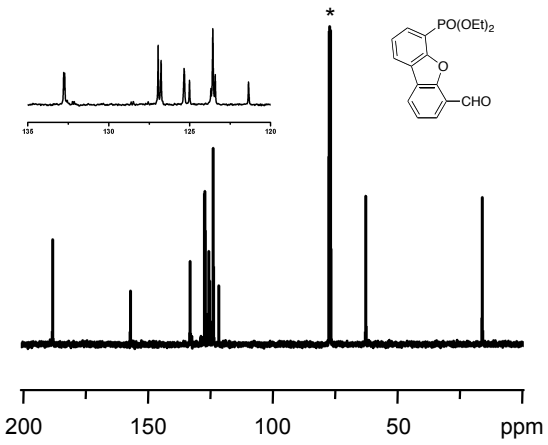

Figure S22. ^{13}C NMR spectrum of 4-formyl-6-diethylphosphonate-dibenzofuran in $CDCl_3$. The solvent residue peak of $CDCl_3$ is labeled (*).

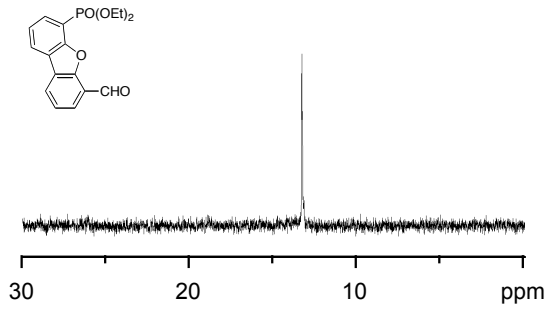

Figure S23. ^{31}P NMR spectrum of 4-formyl-6-diethylphosphonate-dibenzofuran in $CDCl_3$.

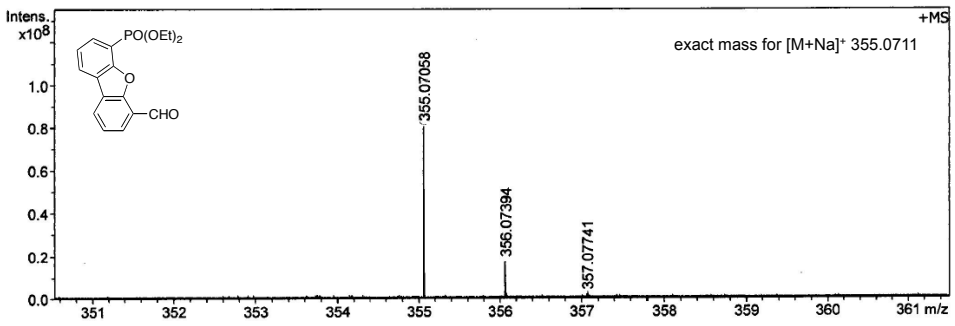

Figure S24. HRMS of 4-formyl-6-diethylphosphonate-dibenzofuran.

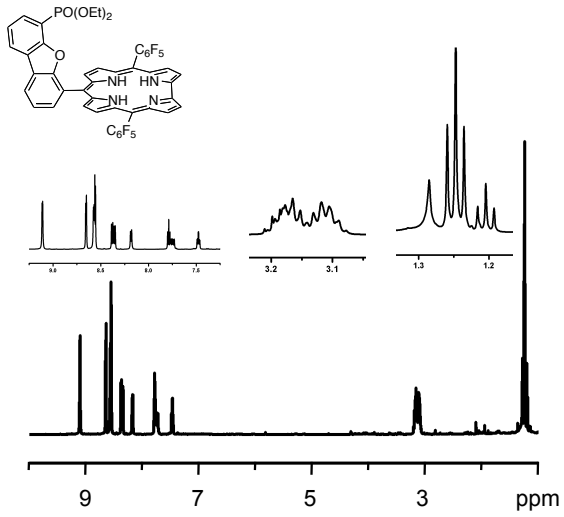

Figure S25. ^{1}H NMR spectrum of $L^{PO(OEt)_2}$ in $CDCl_3$.

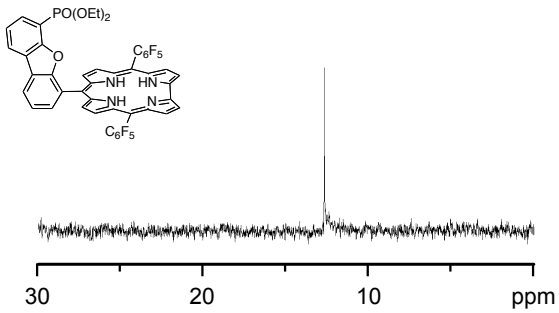

Figure S26. ^{31}P NMR spectrum of $L^{PO(OEt)_2}$ in $CDCl_3$.

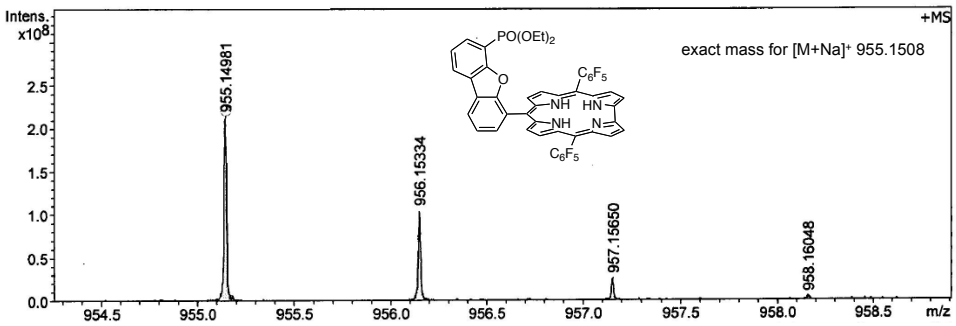

Figure S27. HRMS of $L^{PO(OEt)_2}$.

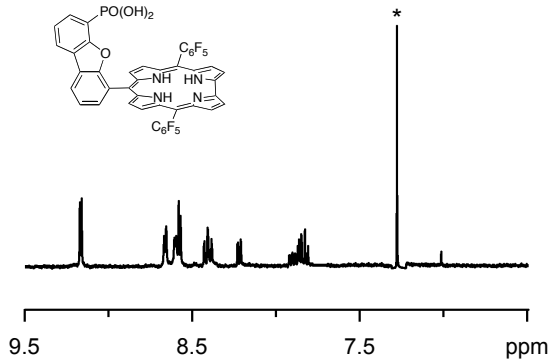

Figure S28. ^{1}H NMR spectrum of $L^{PO(OH)2}$ in $CDCl_3$. The solvent residue peak of $CDCl_3$ is labeled (*).

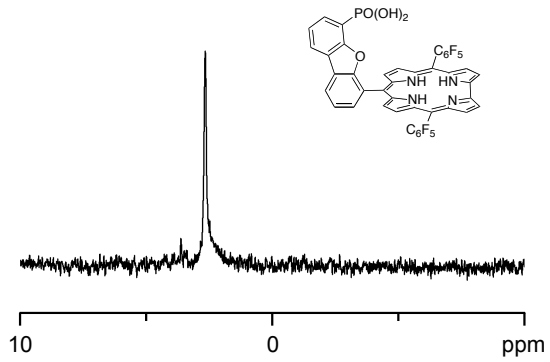

Figure S29. ^{31}P NMR spectrum of $L^{PO(OH)_2}$ in $CDCl_3$.

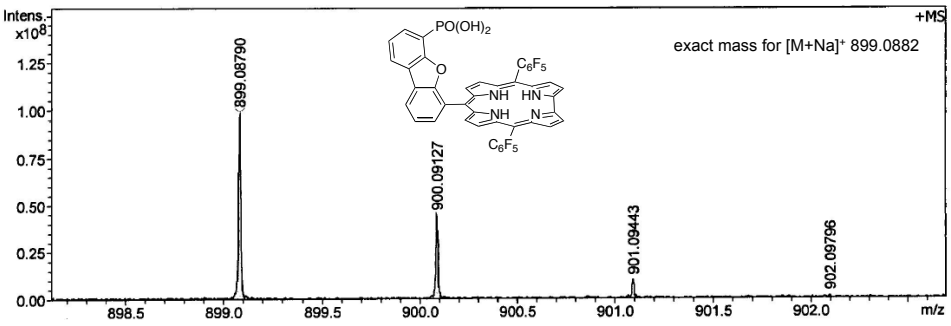

Figure S30. HRMS of $L^{PO(OH)_2}$.

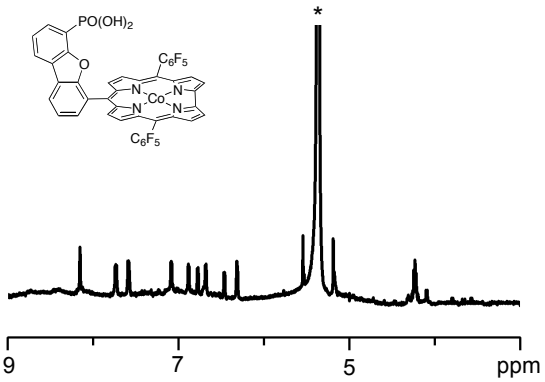

Figure S31. ^{1}H NMR spectrum of $L^{PO(OH)2}$-Co in CD_2Cl_2. The solvent residue peak of CD_2Cl_2 is labeled (*).

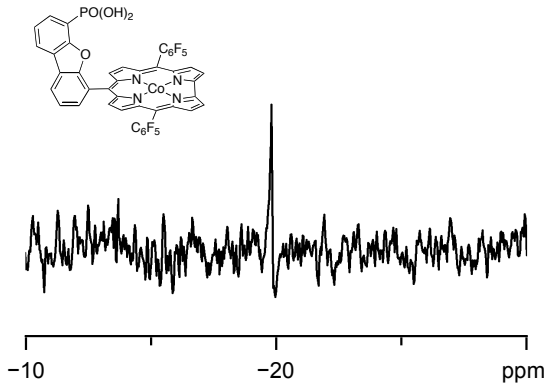

Figure S32. ^{31}P NMR spectrum of $L^{PO(OH)_2}$-Co in CD_2Cl_2.

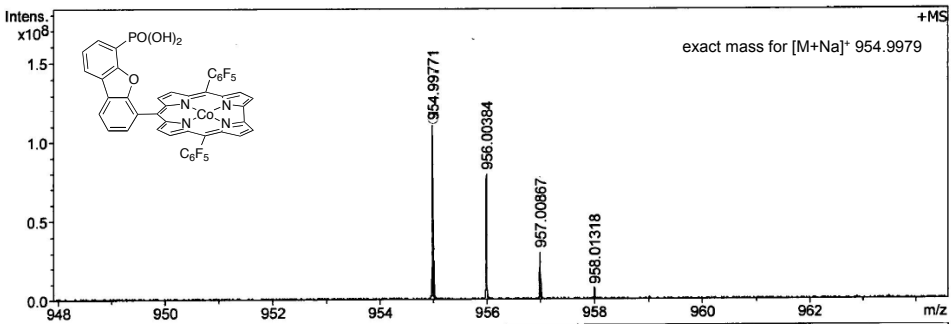

Figure S33. HRMS of $L^{PO(OH)_2}$-Co.

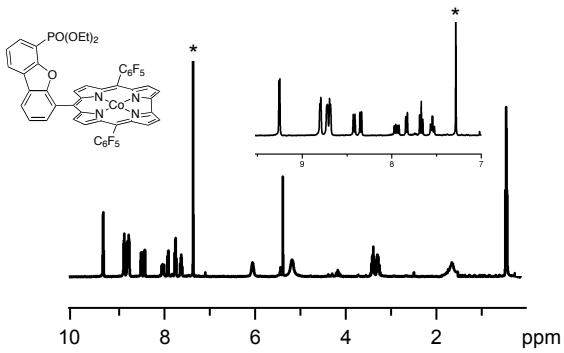

Figure S34. ^{1}H NMR spectrum of $L^{PO(OEt)_2}$-Co in $CDCl_3$. The solvent residue peak of $CDCl_3$ is labeled (*). The peak at 5.31 is due to solvent DCM.

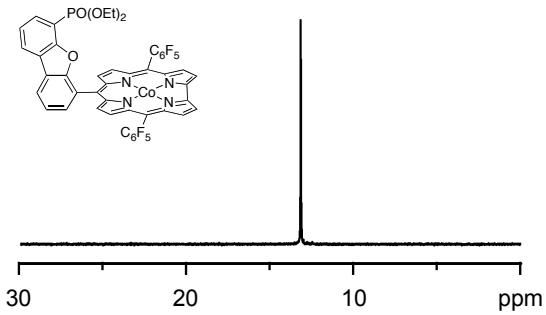

Figure S35. ^{31}P NMR spectrum of $L^{PO(OEt)_2}$-Co in $CDCl_3$.

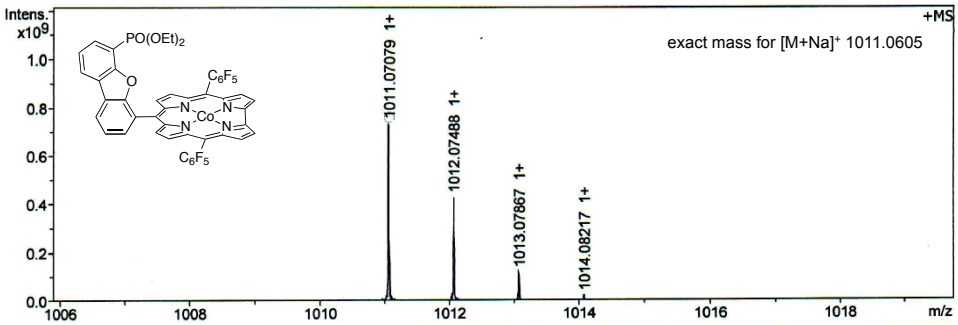

Figure S36. HRMS of $L^{PO(OEt)_2}$-Co.

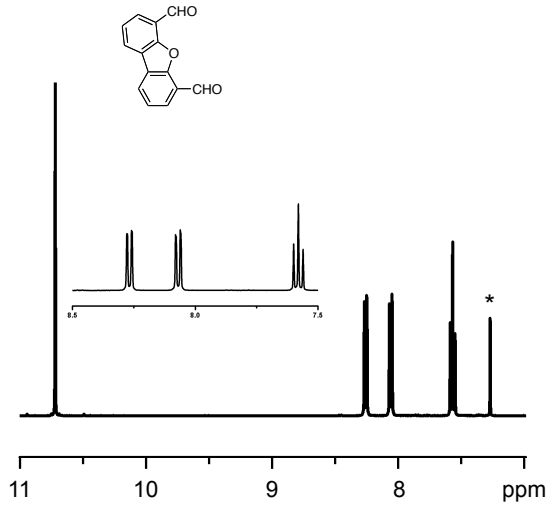

Figure S37. ^{1}H NMR spectrum of 4,6-diformyldibenzofuran in $CDCl_3$. The solvent residue peak of $CDCl_3$ is labeled (*).

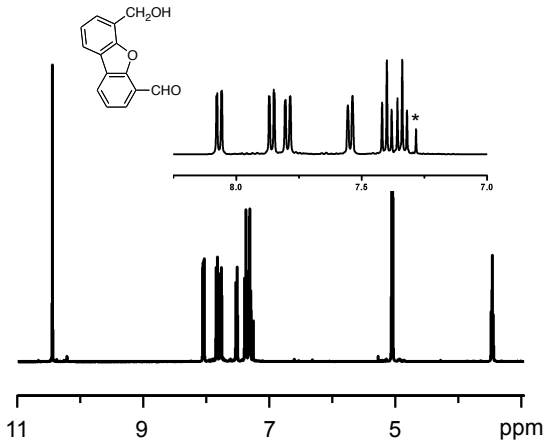

Figure S38. ^{1}H NMR spectrum of 4-formyl-6-hydroxymethyldibenzofuran in $CDCl_3$. The solvent residue peak of $CDCl_3$ is labeled (*).

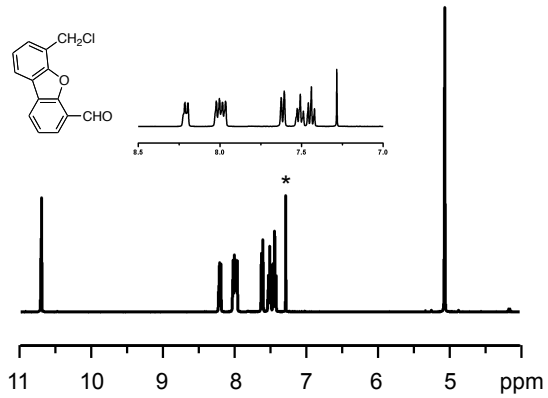

Figure S39. ^{1}H NMR spectrum of 4-formyl-6-chloromethyldibenzofuran in $CDCl_3$. The solvent residue peak of $CDCl_3$ is labeled (*).

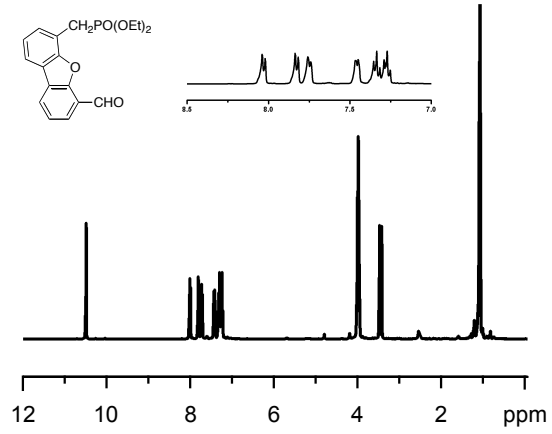

Figure S40. ^{1}H NMR spectrum of 4-formyl-6-diethylphosphatemethyldibenzofuran in $CDCl_3$.

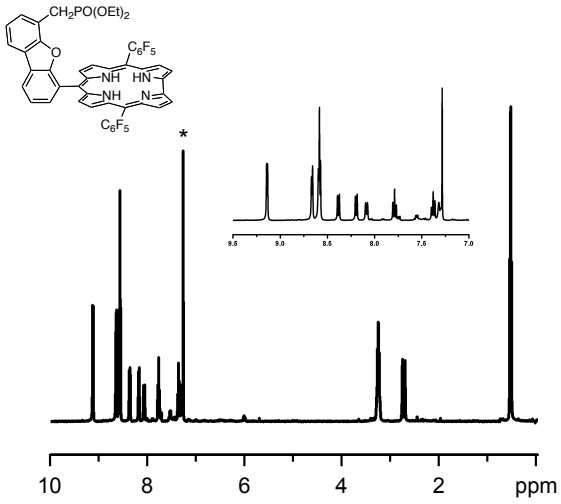

Figure S41. ^{1}H NMR spectrum of $L^{CH_2PO(OEt)_2}$ in $CDCl_3$. The solvent residue peak of $CDCl_3$ is labeled (*).

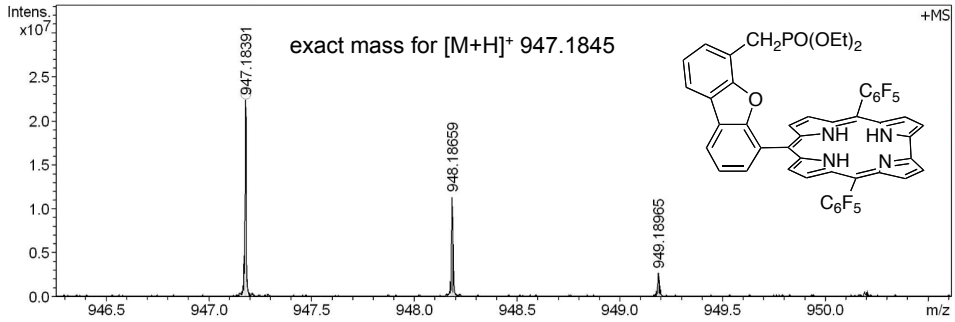

Figure S42. HRMS of $L^{CH_2PO(OEt)_2}$.

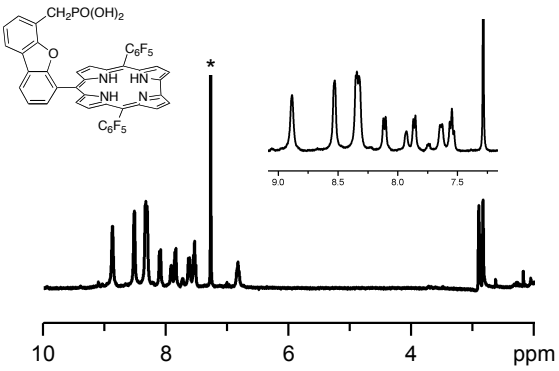

Figure S43. ^{1}H NMR spectrum of $L^{CH_2PO(OH)_2}$ in $CDCl_3$. The solvent residue peak of $CDCl_3$ is labeled (*).

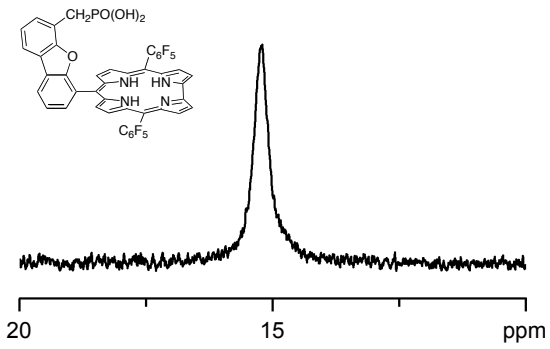

Figure S44. ^{31}P NMR spectrum of $L^{CH_2PO(OH)_2}$ in $CDCl_3$.

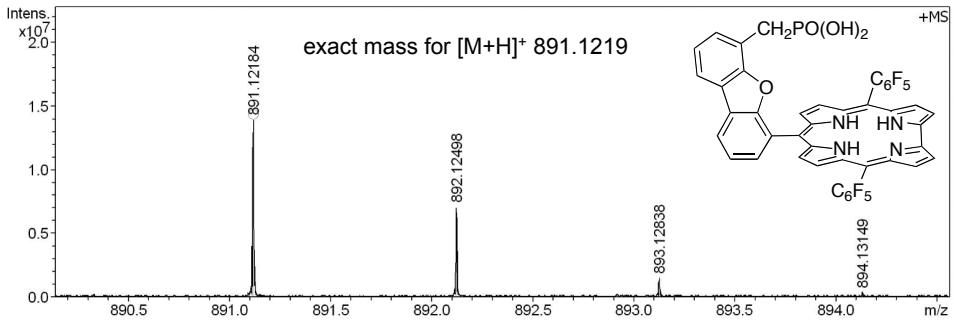

Figure S45. HRMS of $L^{CH_2PO(OH)_2}$.

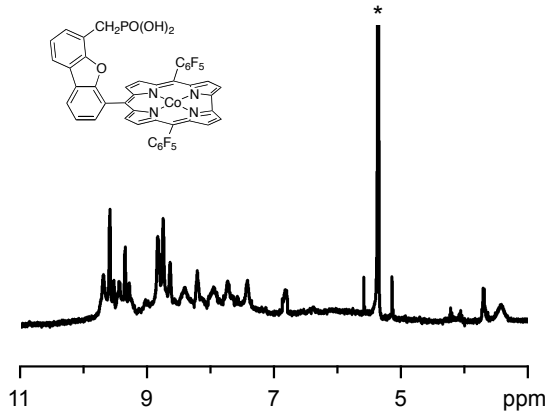

Figure S46. ^{1}H NMR spectrum of $L^{CH_2PO(OH)_2}$-Co in CD_2Cl_2. The solvent residue peak of CD_2Cl_2 is labeled (*).

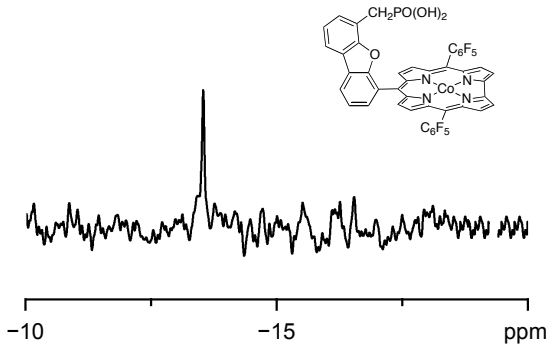

Figure S47. ^{31}P NMR spectrum of $L^{CH_2PO(OH)_2}$-Co in CD_2Cl_2.

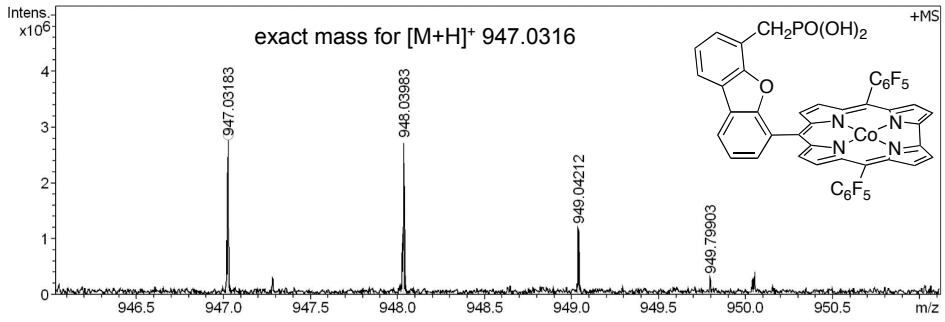

Figure S48. HRMS of $L^{CH_2PO(OH)_2}$-Co.

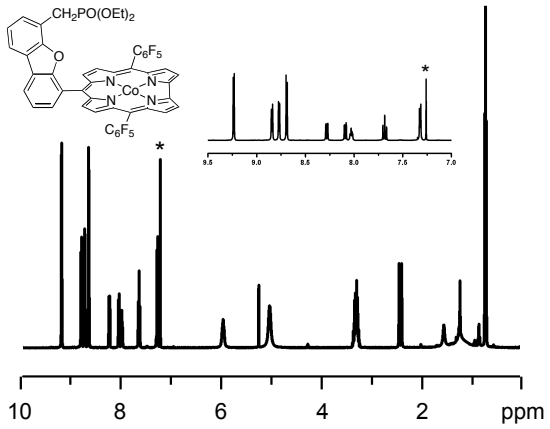

Figure S49. ^{1}H NMR spectrum of $L^{CH_2PO(OEt)_2}$-Co in $CDCl_3$. The solvent residue peak of $CDCl_3$ is labeled (*). The peak at 5.31 is due to solvent DCM.

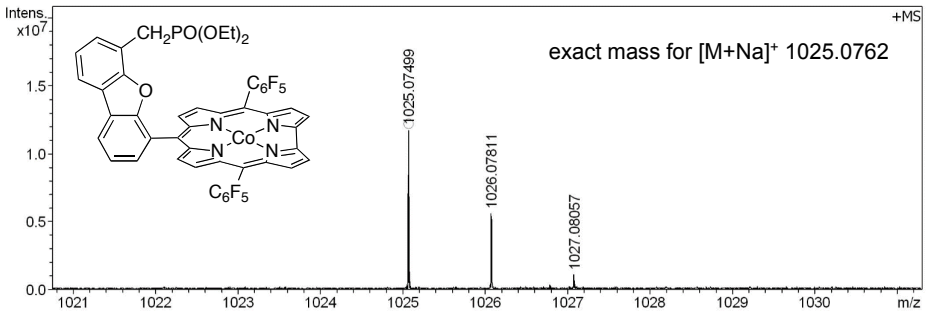

Figure S50. HRMS of $L^{CH_2PO(OEt)_2}$-Co.

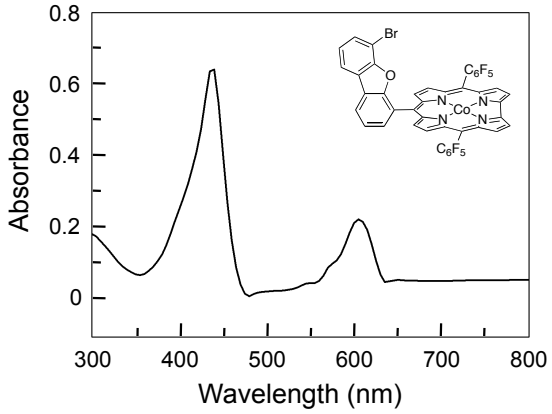

Figure S51. UV-vis spectrum of L^{Br}-Co in DCM at room temperature.

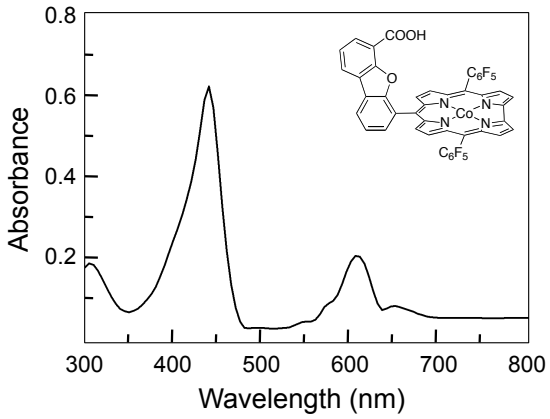

Figure S52. UV-vis spectrum of L^{COOH}-Co in DCM at room temperature.

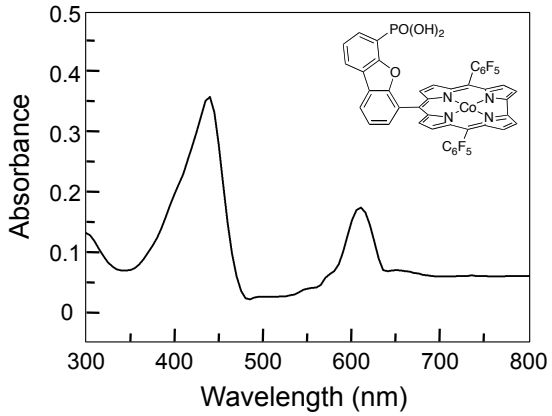

Figure S53. UV-vis spectrum of $L^{PO(OH)_2}$-Co in DCM at room temperature.

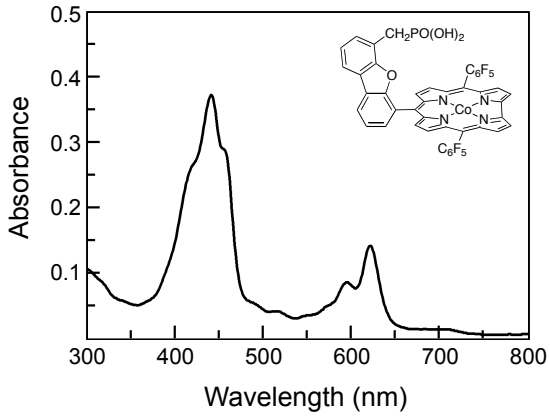

Figure S54. UV-vis spectrum of $L^{CH_2PO(OH)_2}$-Co in DCM at room temperature.

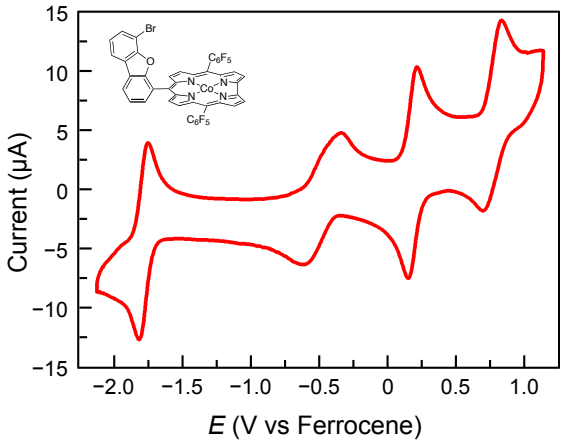

Figure S55. CV of 0.5 mM L^{Br}-Co in acetonitrile. Conditions: 0.1 M *n*-Bu_4NPF_6, GC working electrode, Pt auxiliary electrode, Ag/Ag^+ reference electrode, 50 mV s^{-1} scan rate.

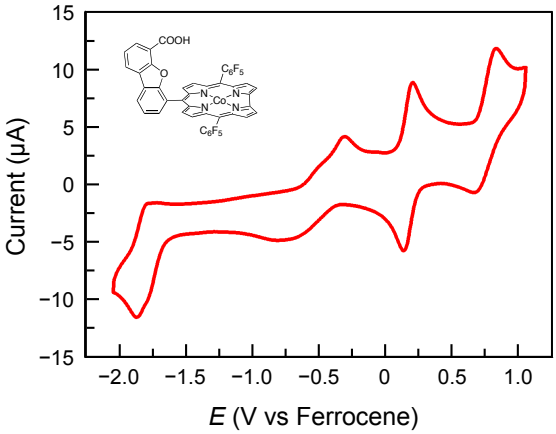

Figure S56. CV of 0.5 mM L^{COOH}-Co in acetonitrile. Conditions: 0.1 M *n*-Bu_4NPF_6, GC working electrode, Pt auxiliary electrode, Ag/Ag^+ reference electrode, 50 mV s^{-1} scan rate.

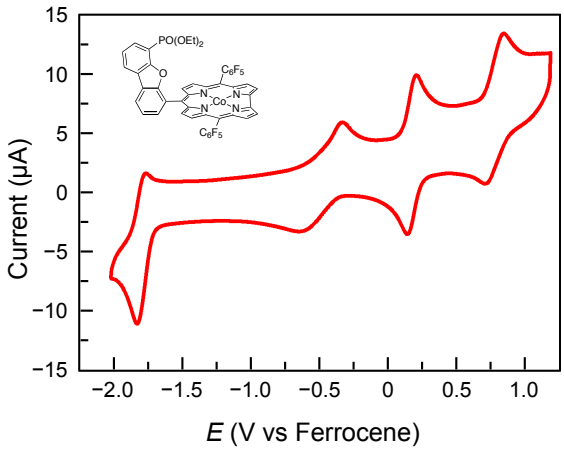

Figure S57. CV of 0.5 mM $L^{PO(OEt)2}$-Co in acetonitrile. Conditions: 0.1 M *n*-Bu_4NPF_6, GC working electrode, Pt auxiliary electrode, Ag/Ag^+ reference electrode, 50 mV s^{-1} scan rate.

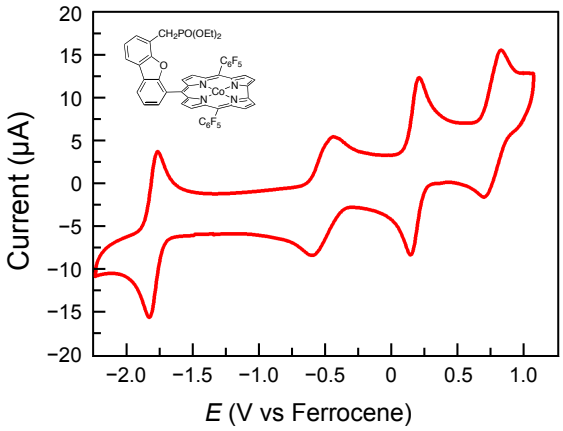

Figure S58. CV of 0.5 mM $L^{CH_2PO(OEt)_2}$-Co in acetonitrile. Conditions: 0.1 M *n*-Bu_4NPF_6, GC working electrode, Pt auxiliary electrode, Ag/Ag^+ reference electrode, 50 mV s^{-1} scan rate.

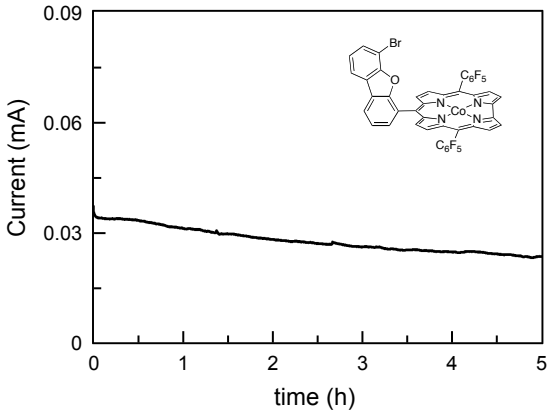

Figure S59. Current profile of controlled potential electrolysis of L^{Br}-Co. Conditions: catalyst-coated FTO working electrode, Pt auxiliary electrode, Ag/AgCl reference electrode, 0.1 M pH 7 phosphate buffer, applied potential 1.5 V, room temperature.

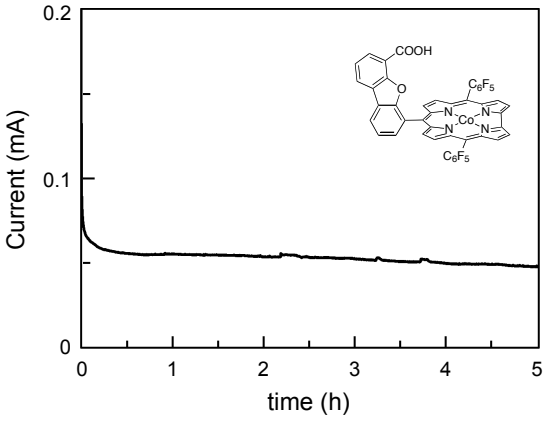

Figure S60. Current profile of controlled potential electrolysis of L^{COOH}-Co. Conditions: catalyst-coated FTO working electrode, Pt auxiliary electrode, Ag/AgCl reference electrode, 0.1 M pH 7 phosphate buffer, applied potential 1.5 V, room temperature.

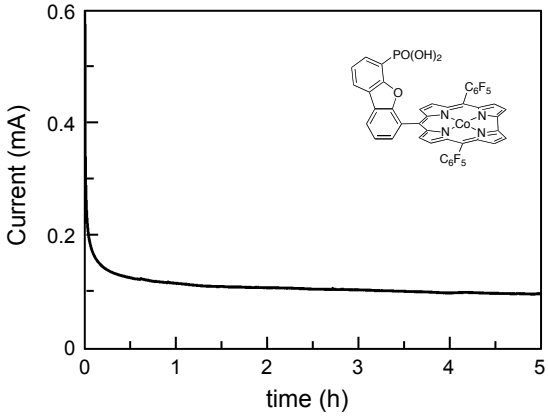

Figure S61. Current profile of controlled potential electrolysis of $L^{PO(OH)_2}$-Co. Conditions: catalyst-coated FTO working electrode, Pt auxiliary electrode, Ag/AgCl reference electrode, 0.1 M pH 7 phosphate buffer, applied potential 1.5 V, room temperature.

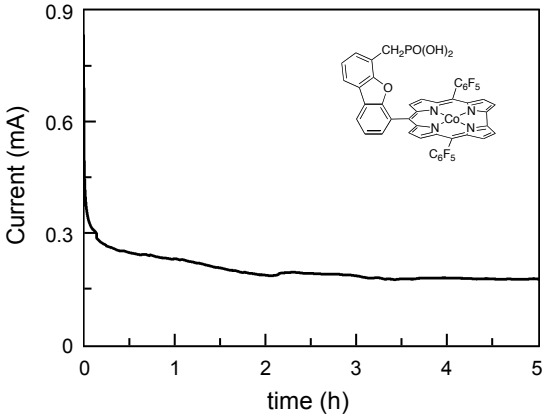

Figure S62. Current profile of controlled potential electrolysis of $L^{CH_2PO(OH)_2}$-Co. Conditions: catalyst-coated FTO working electrode, Pt auxiliary electrode, Ag/AgCl reference electrode, 0.1 M pH 7 phosphate buffer, applied potential 1.5 V, room temperature.

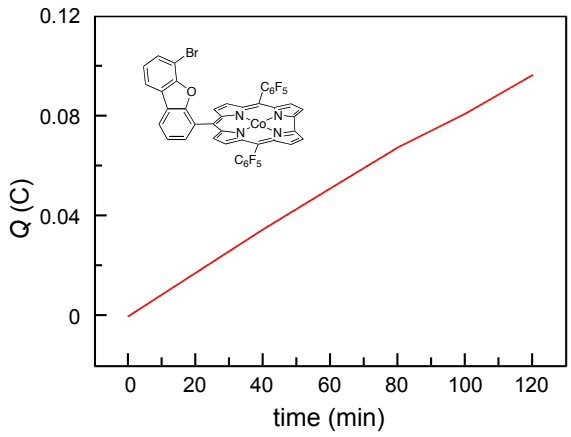

Figure S63. The electric charge curve of the GC electrode coated with L^{Br}-Co during CPE in 0.1 M pH 7.0 phosphate buffer at −1.4 V.

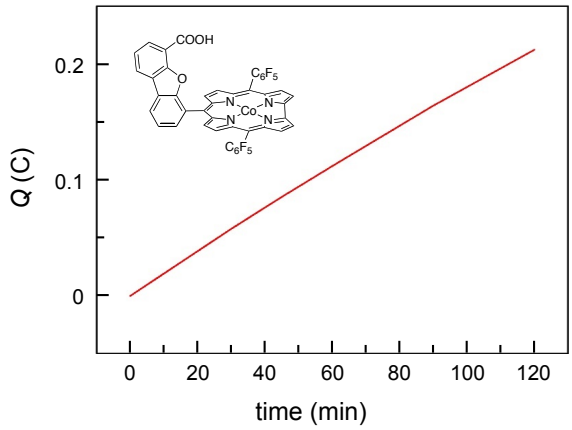

Figure S64. The electric charge curve of the GC electrode coated with L^{COOH}-Co during CPE in 0.1 M pH 7.0 phosphate buffer at −1.4 V.

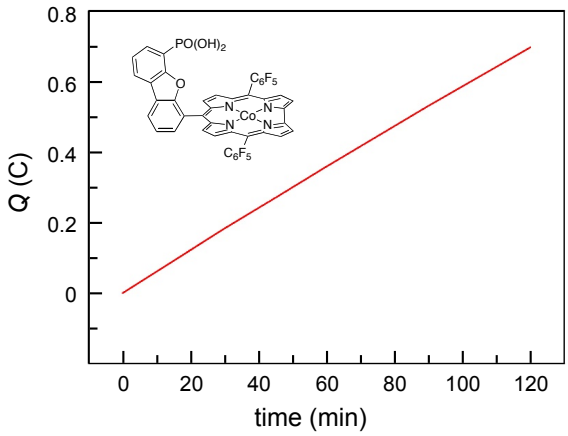

Figure S65. The electric charge curve of the GC electrode coated with $L^{PO(OH)_2}$-Co during CPE in 0.1 M pH 7.0 phosphate buffer at −1.4 V.

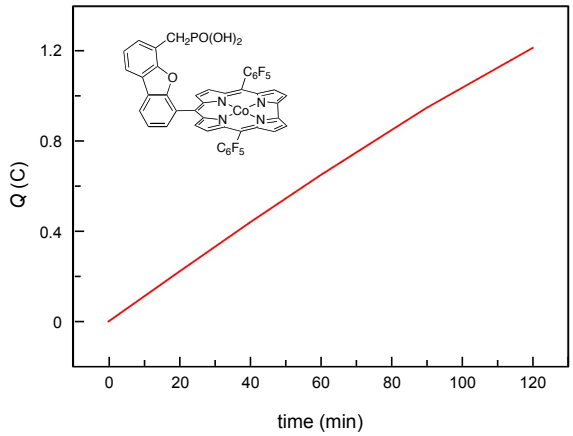

Figure S66. The electric charge curve of the GC electrode coated with $L^{CH_2PO(OH)_2}$-Co during CPE in 0.1 M pH 7.0 phosphate buffer at −1.4 V.

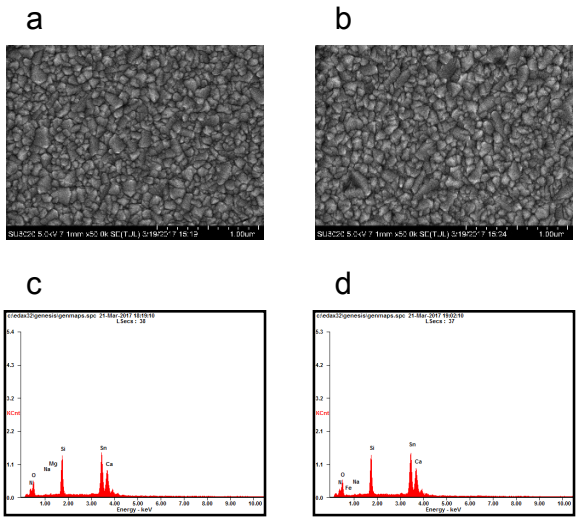

Figure S67. SEM images of FTO electrodes. (a) bare FTO. (b) FTO coated with $L^{CH_2PO(OH)_2}$-Co after CPE and washed by DCM. EDX data for FTO electrodes. (c) bare FTO; (d) FTO coated with $L^{CH_2PO(OH)_2}$-Co after CPE and washed by DCM.

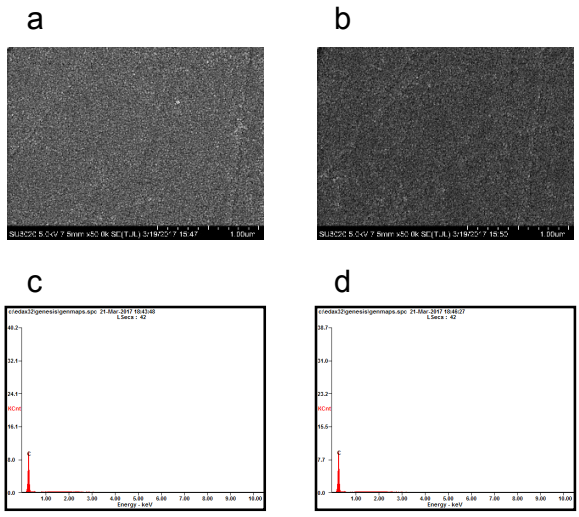

Figure S68. SEM images of GC electrodes. (a) bare GC. (b) GC coated with $L^{CH_2PO(OH)_2}$-Co after CPE and washed by DCM. EDX data for GC electrodes. (c) bare GC; (d) GC coated with $L^{CH_2PO(OH)_2}$-Co after CPE and washed by DCM.

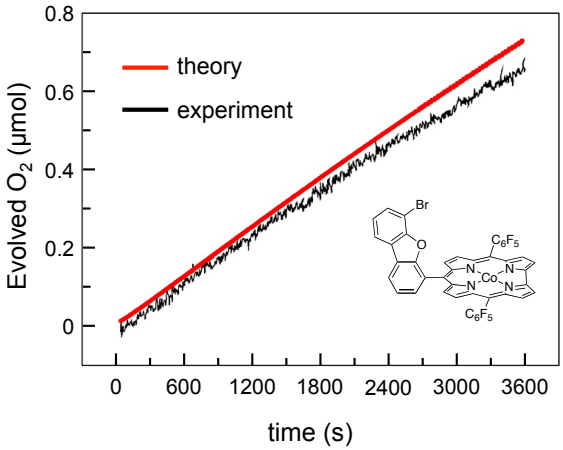

Figure S69. Detection of evolved O_2 during electrolysis at 1.6 V with L^{Br}-Co (black) in 0.1 M pH 7 phosphate buffer and the theoretical amount of O_2 produced (red). The working FTO electrode has an area of 1.0 cm^2 and the catalyst loading is 20 nmol cm^{-2}. Faradaic yield = 91%.

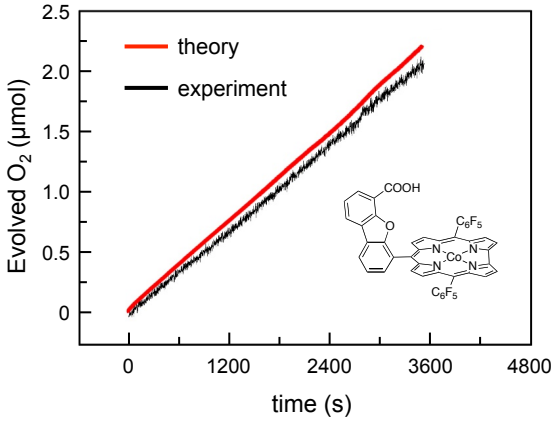

Figure S70. Detection of evolved O_2 during electrolysis at 1.6 V with L^{COOH}-Co (black) in 0.1 M pH 7 phosphate buffer and the theoretical amount of O_2 produced (red). The working FTO electrode has an area of 1.0 cm^2 and the catalyst loading is 20 nmol cm^{-2}. Faradaic yield = 95%.

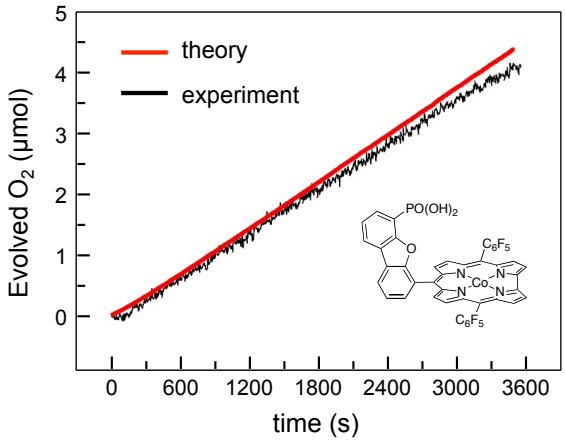

Figure S71. Detection of evolved O_2 during electrolysis at 1.6 V with $L^{PO(OH)_2}$-Co (black) in 0.1 M pH 7 phosphate buffer and the theoretical amount of O_2 produced (red). The working FTO electrode has an area of 1.0 cm^2 and the catalyst loading is 20 nmol cm^{-2}. Faradaic yield = 95%.

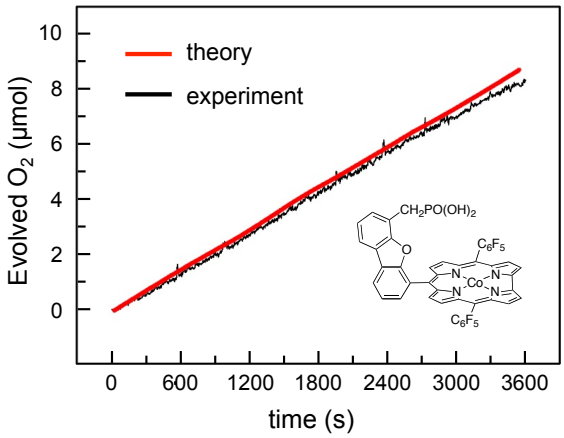

Figure S72. Detection of evolved O_2 during electrolysis at 1.6 V with $L^{CH_2PO(OH)_2}$-Co (black) in 0.1 M pH 7 phosphate buffer and the theoretical amount of O_2 produced (red). The working FTO electrode has an area of 1.0 cm^2 and the catalyst loading is 20 nmol cm^{-2}. Faradaic yield = 96%.

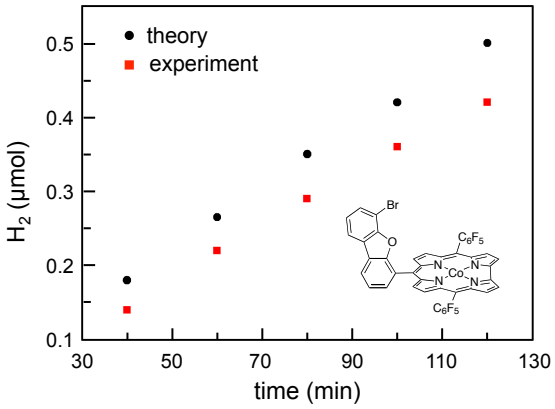

Figure S73. Gas chromatography detection of evolved H_2 during electrolysis with L^{Br}-Co (red) and theoretical amount of H_2 produced (black) at −1.4 V. Electrolysis conditions: 0.1 M pH 7.0 phosphate buffer. Faradaic yield = 78%.

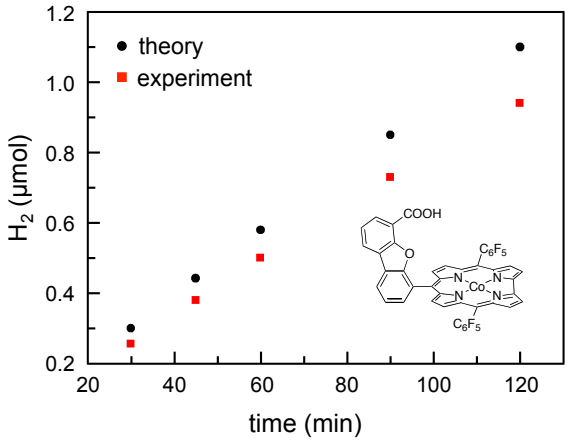

Figure S74. Gas chromatography detection of evolved H_2 during electrolysis with L^{COOH}-Co (red) and theoretical amount of H_2 produced (black) at −1.4 V. Electrolysis conditions: 0.1 M pH 7.0 phosphate buffer. Faradaic yield = 80%.

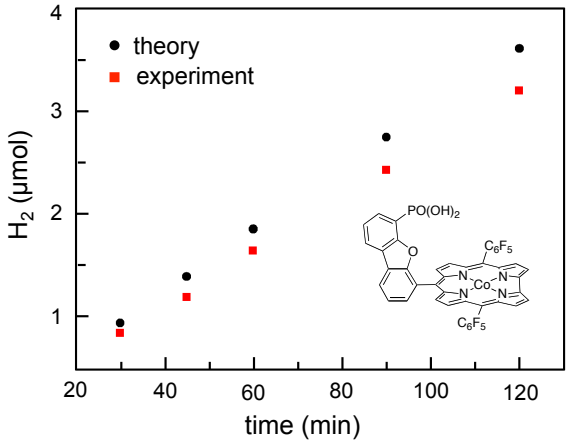

Figure S75. Gas chromatography detection of evolved H_2 during electrolysis with $L^{PO(OH)_2}$-Co (red) and theoretical amount of H_2 produced (black) at −1.4 V. Electrolysis conditions: 0.1 M pH 7.0 phosphate buffer. Faradaic yield = 87%.

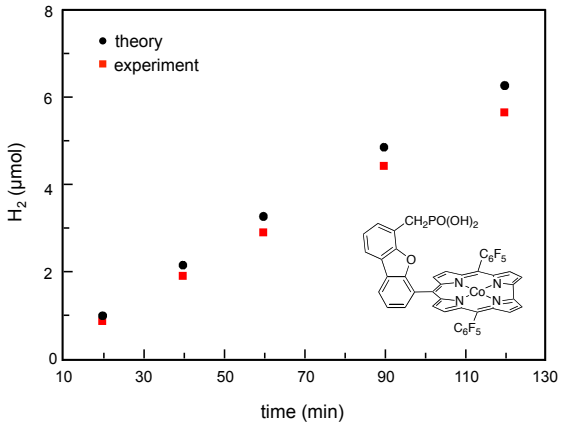

Figure S76. Gas chromatography detection of evolved H_2 during electrolysis with $L^{CH_2PO(OH)_2}$-Co (red) and theoretical amount of H_2 produced (black) at −1.4 V. Electrolysis conditions: 0.1 M pH 7.0 phosphate buffer. Faradaic yield = 94%.

Table S1. Crystal data and structure refinement parameters.

Complex	$L^{CH_2PO(OEt)_2}$-Co	$L^{PO(OEt)_2}$
molecular formula	$C_{58.35}H_{36.70}Cl_{0.70}CoF_{10}N_6O_4P$	$C_{53}H_{41}F_{10}N_4O_4P$
formula wt. (g mol^{-1})	1190.55	1018.87
temperature (K)	150(2)	173(2)
radiation (λ, Å)	0.71073	0.71073
crystal system	orthorhombic	orthorhombic
space group	$P2_12_12$	Pbca
a (Å)	16.990(8)	10.065(2)
b (Å)	35.806(16)	29.201(6)
c (Å)	8.617(4)	32.249(6)
Volume (Å^3)	5242(4)	9478(3)
Z	4	8
ρ_{calcd} (g cm^{-3})	1.508	1.428
μ (mm^{-1})	0.485	0.149
F(000)	2419	4192
crystal size (mm^3)	0.50 × 0.20 × 0.05	0.42 × 0.19 × 0.17
Theta range	2.36 to 21.96°	1.26 to 23.26°
reflections collected	16666	25282
independent reflections	5495 [R(int) = 0.0618]	6793 [R(int) = 0.0469]
Completeness	92.0%	99.7%
goodness-of-fit on F^2	1.083	1.034
final R indices	$R1^a$ = 0.0558	$R1^a$ = 0.0870
[R > 2σ (I)]	wR_2^b = 0.1298	wR_2^b = 0.2225
R indices (all data)	$R1^a$ = 0.0684	$R1^a$ = 0.1023
	wR_2^b = 0.1392	wR_2^b = 0.2453
largest diff. peak and hole (e Å^{-3})	0.657 and −0.391	0.890 and −0.729

$^aR_1 = \Sigma||F_o| - |F_c|| / |F_o|$, $^bwR_2 = \{\Sigma[w(F_o^2 - F_c^2)^2] / \Sigma[w(F_o^2)^2]\}^{0.5}$

Table S1. Crystal data and structure refinement parameters (continued).

Complex	L^{COOMe}	L^{Br}-Co-PPh_3
molecular formula	$C_{45}H_{20}F_{10}N_4O_3$	$C_{61}H_{29}BrCoF_{10}N_4OP$
formula wt. (g mol^{-1})	854.65	1193.69
temperature (K)	173(2)	150(2)
radiation (λ, Å)	0.71073	0.71073
crystal system	triclinic	orthorhombic
space group	$P\bar{1}$	*P*bca
a (Å)	15.525(3)	12.4310(7)
b (Å)	16.113(3)	27.8731(15)
c (Å)	17.383(4)	28.7605(14)
α (°)	105.88(3)	
β (°)	101.79(3)	
γ (°)	107.16(3)	
Volume ($Å^3$)	3799.2(13)	9965.2(9)
Z	4	8
ρ_{calcd} (g cm^{-3})	1.494	1.591
μ (mm^{-1})	0.129	1.266
F(000)	1728	4784
crystal size (mm^3)	0.19 × 0.18 × 0.16	0.60 × 0.50 × 0.28
Theta range	1.60 to 27.48°	2.29 to 26.40°
reflections collected	46794	74368
independent reflections	17371 [R(int) = 0.0559]	10153 [R(int) = 0.0418]
Completeness	99.7%	99.3%
goodness-of-fit on F^2	1.091	1.040
final R indices	$R1^a$ = 0.0876	$R1^a$ = 0.0342
[R > 2σ (I)]	wR_2^b = 0.2278	wR_2^b = 0.0830
R indices (all data)	$R1^a$ = 0.1074	$R1^a$ = 0.0467
	wR_2^b = 0.2434	wR_2^b = 0.0886
largest diff. peak and hole (e $Å^{-3}$)	0.526 and −0.469	0.544 and −0.772

$^aR_1 = \Sigma||F_o| - |F_c|| / |F_o|$, $^bwR_2 = \{\Sigma[w(F_o^2 - F_c^2)^2] / \Sigma[w(F_o^2)^2]\}^{0.5}$

Table S2. The amount of loaded catalysts (based on Co) as determined by ICP-AES.

Catalyst	GC (nmol cm^{-2})	FTO (nmol cm^{-2})
L^{Br}-Co	76.8	20.7
L^{COOH}-Co	72.3	19.8
$L^{PO(OH)_2}$-Co	75.1	20.5
$L^{CH_2PO(OH)_2}$-Co	68.1	19.0

Table S3. The redox potentials of the four Co corroles as determined in acetonitrile.

Complex	$E_{1/2}$[a] (V vs ferrocene)			
	2nd oxidation	1st oxidation	1st reduction	2nd reduction[b]
L^{Br}-Co	0.76	0.18	−0.47	−1.79
L^{COOH}-Co	0.76	0.17	−0.52	−1.83
$L^{PO(OEt)_2}$-Co	0.78	0.17	−0.48	−1.80
$L^{CH_2PO(OEt)_2}$-Co	0.77	0.18	−0.52	−1.79

[a]Samples dissolved in acetonitrile (0.1 M Bu_4NPF_6) were measured at 50 mV s^{-1} scan rate. [b]For L^{COOH}-Co, because of the presence of proton reduction, the redox is irreversible, and thus $E_{p,c}$ is reported.

References

1. E. B. Schwartz, C. B. Knobler and D. J. Cram, *J. Am. Chem. Soc.*, 1992, **114**, 10775-10784.
2. W. G. Skene, V. Berl, H. Risler, R. Khoury and J. M. Lehn, *Org. Biomol. Chem.*, 2006, **4**, 3652-3663.
3. *APEX2 v2009*, Bruker AXS., Madison, WI, 2009.
4. G. M. Sheldrick, *SADABS, 2008/1*, University of Göttingen, Göttingen, Germany, 2008.
5. G. M. Sheldrick, *Acta Cryst.*, 1990, **A46**, 467-473.
6. G. M. Sheldrick, *Acta Cryst.*, 2008, **A64**, 112-122.